OPTIMIZED UPPER BOUND ANALYSIS OF POLYMER COATED METAL ROD EXTRUSION THROUGH CONICAL DIE

A Thesis

by

RITESH LALIT SHAH

Submitted to the Office of Graduate Studies of
Texas A&M University
in partial fulfillment of the requirements for the degree of

MASTER OF SCIENCE

May 2006

Major Subject: Mechanical Engineering

OPTIMIZED UPPER BOUND ANALYSIS OF POLYMER COATED METAL ROD EXTRUSION THROUGH CONICAL DIE

A Thesis

by

RITESH LALIT SHAH

Submitted to the Office of Graduate Studies of
Texas A&M University
in partial fulfillment of the requirements for the degree of

MASTER OF SCIENCE

Approved by:

Chair of Committee,	Jyhwen Wang
Committee Members,	Richard Alexander
	Don T. Phillips
Head of Department,	Dennis O' Neal

May 2006

Major Subject: Mechanical Engineering

ABSTRACT

Optimized Upper Bound Analysis of Polymer Coated Metal Rod Extrusion Through Conical Die. (May 2006)

Ritesh Lalit Shah, B. E., College of Engineering, Pune, India

Chair of Advisory Committee: Dr. Jyhwen Wang

Extrusion is a metal forming process used extensively in industry to produce different structural, mechanical, electrical, architectural, automotive and aerospace application parts. Currently after extrusion, the rod is subjected to environmental wear due to long storage time and hence requires an additional cleaning process before further use. This cleaning process can be eliminated by extruding a polymer coated metal rod workpiece such that the polymer coating is sustained on the final product after the extrusion process.

In the present research study a new upper bound analytical model is developed to predict the forces required to conduct extrusion of a polymer coated metal rod successfully. The search for the lower upper bound power functional is modeled as a non linear optimization problem. Optimizing the functional also determines the set of constraints defining the shape of rigid plastic deformation boundaries and the final coating thickness. Also an upper bound analytical model was developed to predict forces for failure of the polymer coating during the extrusion. Both the analytical models for

successful and failed extrusion are compared to obtain critical die angle which can provide tooling and process design guidelines. Finite element analysis simulations were modeled using commercially available software package, ABAQUS. Predictions of FEA simulations were in good agreement with published results and with the predictions of analytical model developed in this study.

Dedicated to my mother, Tara Shah, and father, Lalit Shah, for all their love, encouragement and support throughout my life, for which I am eternally grateful. Without them, this would not have been possible.

ACKNOWLEDGEMENTS

It gives me immense pleasure to express my deepest appreciation to Dr. Jyhwen Wang for giving me the opportunity to work on this research project and for his invaluable advice, guidance and support throughout the thesis while allowing me the room to work in my own way. Thank you for keeping patience with me and constantly inspiring me to achieve my academic goals.

I would also like to express gratitude to Dr. Richard Alexander for providing constructive comments, suggestions and improving my technical writing skills, which would be an asset in my future endeavors. I also thank Dr. Don T. Phillips for serving on my thesis committee and for always being ready to go through any formalities.

Finally I would like to acknowledge the services of all the people who have helped me directly or indirectly from Texas A&M University to complete my research.

TABLE OF CONTENTS

Page

Page

LIST OF FIGURES

FIGURE Page

LIST OF TABLES

NOMENCLATURE

ϕ	streamline function or flow function for plastic flow
η	parameter constant along a streamline
$f(\eta)$	function of η and equal to stream function
a	coefficient of parameter η
ϕ_m, ϕ_p	flow functions for metal and polymer, respectively
η_m, η_p	parameters constant along streamline for metal and polymer, respectively
a_{1m}, a_{1p}	coefficient of parameter η for metal and polymer respectively
r, θ, z	coordinates of cylindrical coordinate system
α	semi cone angle of conical die
γ	half angle of interface boundary between metal and polymer
$R_m(z)$	function along the interface of metal and polymer
$R_p(z)$	conical die profile function
Γ_{mi}, Γ_{mf}	rigid-plastic boundary function for metal at entry and exit of die, respectively
Γ_{pi}, Γ_{pf}	rigid-plastic boundary function for polymer at entry and exit of die, respectively
V_i, V_f	velocity of billet at entry and exit of die, respectively
R	vertical position coordinate for rigid-plastic boundaries
L	horizontal position coordinate for rigid-plastic boundaries

V_r, V_θ, V_z	velocity component in r, θ and z direction, respectively
$(\,)'$	derivative of term ( ) with respect to z
$\lvert\Delta V\rvert_\Gamma$	velocity discontinuity along rigid-plastic boundary
$\lvert\Delta V\rvert_{R_p}$	velocity discontinuity along die surface
$\lvert\Delta V\rvert_{R_m}$	velocity discontinuity along interface boundary of metal and polymer
$\dot{\varepsilon}_{ij}$	components of strain rate tensor
U	Displacement
$\dot{W}_i, \dot{W}_s, \dot{W}_f$	power dissipation due to internal deformation, internal shear and friction, respectively
$\bar{\sigma}$	effective stress
$\dot{\bar{\varepsilon}}$	effective strain
σ_0	flow stress of material
J	total power by upper bound method
m	Friction
V_{AB}, V_{BC}, V_{AC}	tangential velocity along shear planes AB, BC and AC, respectively
V_o	velocity of the outgoing shaved polymer coating
t_i	initial thickness of polymer coating
t_o	thickness of outgoing shaved polymer coating
$L_{CD}, L_{AB}, L_{AC}, L_{BC}$	length of shear planes CD, AB, AC and BC respectively,

Subscripts

m	metal layer
p	polymer layer
i	entry of die
f	exit of die

CHAPTER I

INTRODUCTION

Since last few decades, much effort has been devoted to develop plasticity theories to understand the mechanics underlying metal forming processes in better manner as these processes have played a phenomenal role in shaping the innumerous products that we use today. Among the various forming processes in existence, extrusion is a vital forming process and is used extensively in industry to produce different structural, mechanical, electrical, architectural, automotive and aerospace application parts.

Extrusion is a forming process, which consists of material flow through confined and converging dies to change the size and/or shape of the original billet. Axisymmetric extrusion means that both the deformation process and outgoing product is symmetric in shape about the central axis and is used mostly to produce rods and wires in industry. Composite rod extrusion or polymer coated metal rod extrusion produces a thin polymer coating on an extruded metal rod.

The thesis follows the style and format of ASME Journal of Manufacturing Science and Engineering.

1.1 Polymer coatings

In general a composite material is made up of two or more different materials to achieve desired structural properties or cost effectiveness. As composites replace conventional materials in more and more applications, production of composite materials by metal forming processes has become an important subject to study. Due to their low coefficient of friction, use of polymers as an intermediate lubricant in metal forming operations such as deep drawing and extrusion is well known and explored by Schey [1], Rao [2] and Mear et. al. [3]. Good lubrication properties of plastics allow reducing critical loads required for deformation process. Other advantages of using polymer coating over metal rod during extrusion can provide surface protection against general damage, corrosion and chemical attack. This is due to the fact that polymers have good ductility and good corrosion resistance from most chemical agents.

There are several industrial applications of polymer coating on metal rods in industry and a real life scenario is explained next. Rods or billets, produced by axisymmetric extrusion, are stored in warehouse for weeks before actually being used to make final products by further processing. Due to moisture and other elements present in the environment, the surface of the rods may be corroded or damaged. Before using the rod or billet for further processing, it has to undergo some cleaning operation like pickling and subsequent washing, which is time consuming and cost ineffective, since it does not

add any value to the final product. Hence, one viable solution is to produce rods or billets with a polymer coating which will protect it against all such damages.

There are various methods used to apply polymer coating to a metal substrate and the method of choice depends on many factors like coating thickness required, production rate and cost optimization, size and shape of the part, and environmental requirements may also play an important role. Various methods used to apply polymer coating are adhesives, vapor deposition, hot dipping, spray coating, immersion coating or powder coating.

While selecting the polymer to be used as a coating, there are some important parameters to be considered. Polymers are made of long chains of molecules and are classified into thermoplastics and thermosets. Thermoplastics have no bonding between molecules whereas thermosets have strong intermolecular bonding. Just like metals, thermoplastic polymers also have melting point (T_m), where phase transforms from solid to liquid. But for polymers there is another important temperature called the glass transition temperature (T_g), which is far more important than the melting point temperature for considering the polymer's use in an application for the reasons summarized below.

Many mechanical and physical properties change drastically when temperature approaches the glass transition temperature, T_g, such as modulus of elasticity, viscosity, coefficient of diffusion and light refraction index. Figure 1 shows the change in modulus

with temperature for a typical thermoplastic. Below the glass transition temperature thermoplastics act as elastic brittle solids and are unable to deform plastically and thus are not suitable for use as coating. Above the glass transition temperature, thermoplastics show low elastic modulus and high deformability. Hence they should be operated above the glass transition temperature, T_g, for forming operations. Thermoplastics become increasingly soft and viscous and behave more like a viscous fluid as the temperature approaches the melting point. Use of Polyethylene (PE) or Polypropylene (PP) can be considered as a coating material, since their glass transition temperatures are below room temperature.

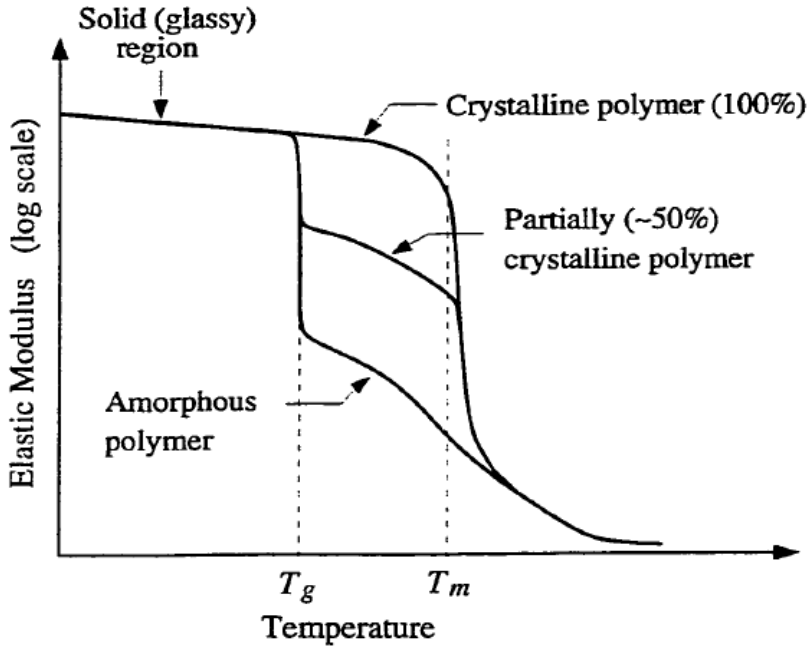

Fig. 1 Typical mechanical properties for a thermoplastic [4]

1.2 Composite rod extrusion

During composite rod extrusion a metal rod of particular initial diameter having a thin polymer coating is forcefully passed through conical die to form an elongated metal rod with reduced final diameter and coating thickness. Since the process is axisymmetric, the cross section remains unchanged in shape and the final product is also axisymmetric. During the process of extrusion the metal and polymer both undergo plastic deformation. Figure 2 shows successful axisymmetric extrusion of a polymer coated metal rod. Successful axisymmetric extrusion of a polymer coated metal rod depends on the optimum combination of following parameters - die angle, reduction ratio, coating thickness, initial velocity and friction, apart from proper tool geometry (such as die length, fillet radius etc.) and material properties.

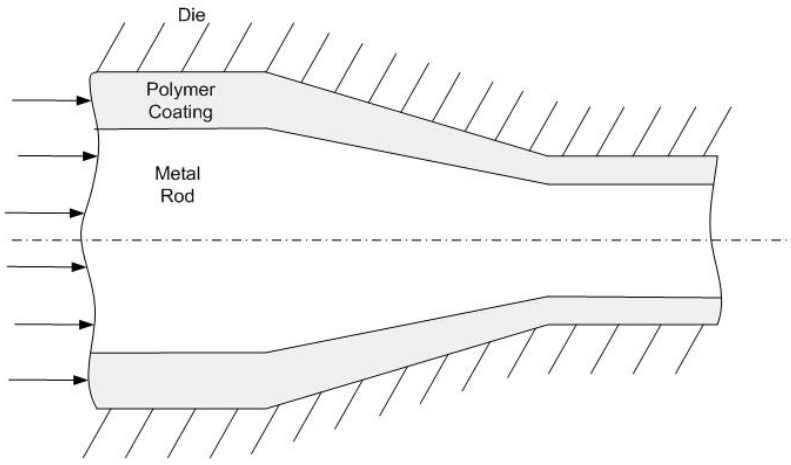

Fig. 2 Successful extrusion of polymer coated metal rod

1.3 Defects in composite rod extrusion

An important concern in metal forming processes is whether the desired deformation can be accomplished without fracture of the workpiece. Even though several studies have been performed on the polymer coating as an intermediate lubricant film during extrusion; but survivability and formability of polymer coating layer on the final product is not given much attention before. In fact, little research has been done to study bonded polymer coatings as a lubricant and much development work devoted to bonded polymer coatings is still needed [1]. Adhesive forces between the polymer and metal depend on the method used to deposit the polymer layer on the metal, but the forces are primarily due to weak Van der Waals attraction force. On the other hand cohesive forces in polymers are due to stronger covalently bonded structure among its monomer chains. Hence predicting adhesive failure of polymer is as important, if not more, than predicting cohesive failure. Following are the most likely failure cases which might occur during axisymmetric extrusion of a polymer coated metal rod.

1.3.1 Center bursting or chevroning

Center bursting or chevroning, as it is also called, is the presence of voids in the material in a repetitive manner along the center line of the final product with no visible defects at the surface as shown in Figure 3. Avitzur [5] was the first to develop an analytical model to predict the center bursting defect in axisymmetric extrusion of single material. During

composite rod extrusion the same defect could occur with the polymer being intact and center burst defect present at the center of the core metal. This defect in composite rod extrusion is more harmful than surface fracture since visually there is no sign of the underlying defect at the surface. Figure 4 below shows a hypothetical failure of center bursting for polymer coated metal rod extrusion.

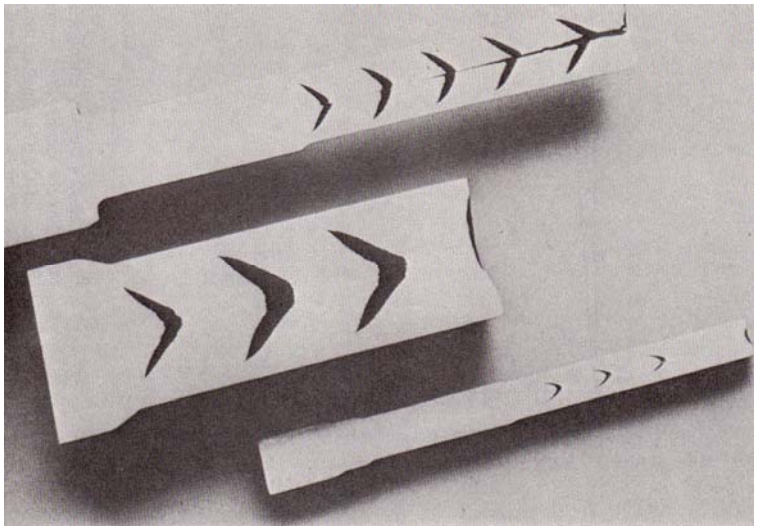

Fig. 3 Center bursting in extruded steel rods Hosford et. al. [6]

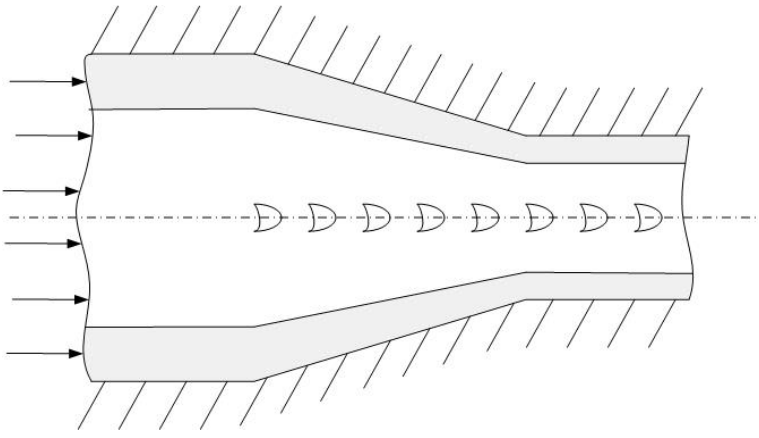

Fig. 4 Center bursting or chevroning defect in composite rod extrusion

1.3.2 Cohesive failure of polymer coating

As the polymer coated metal rod is extruded it undergoes plastic deformation due to shear stresses developed within the material. The outermost layer of the polymer experiences the higher strain rates as compared to the inner layers or central layer and hence it is more likely to fail under these stresses. Hence, high stresses in the outer layers of polymer coating might initiate a crack at the surface which would propagate to the inner layer. Cohesive failure can be recognized visually as the intermittent absence of polymer coating on the metal rod in the final product, as shown in Figure 5. Thus, during cohesive failure the final product has bare core metal rod at places and has polymer coating at other places, which is obviously not the desired result. Clift [7] did pioneering work in predicting fracture during various metal forming processes; for axisymmetric extrusion he found criteria developed by Cockroft [8] to be more suitable for predicting the ductile fracture.

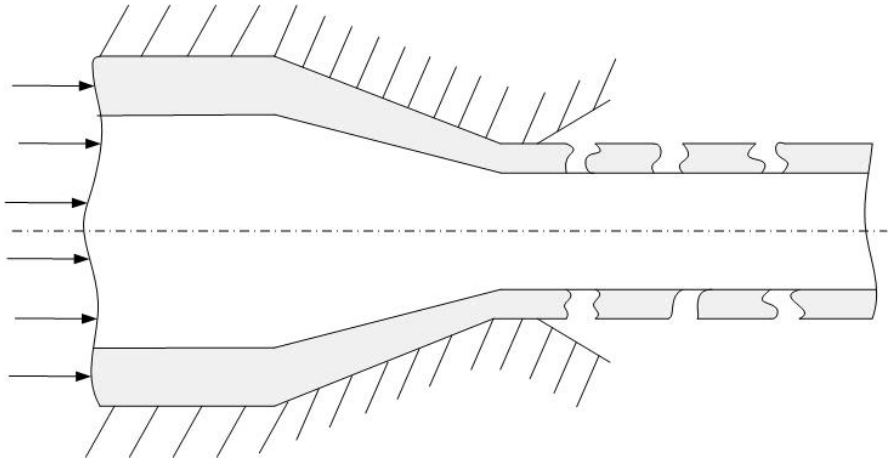

Fig. 5 Cohesive failure of polymer coating during composite rod extrusion

1.3.3 Adhesive failure of polymer coating

Due to difference in yield strength and stress-strain relationship of metal and polymer, each material undergoes a different plastic deformation during extrusion. Obviously polymers have lower yield strength and hence they experience larger strains as compared to the core metal rod. The ratio of polymer coating thickness to the radius of metal rod would not be in exact proportion before and after the extrusion. If the final coating thickness is less than the value derived from proportion of initial coating thickness to initial radius of metal rod, the exit velocity of the polymer will be greater than that of the metal and the polymer will has a tendency to rush ahead of the metal at the exit end of die. If the difference in exit velocities is large enough, it may overcome the adhesive force between the metal and polymer and the polymer coating might fail. In this type of failure, the final product is bare metal rod with no coating, as shown in Figure 6.

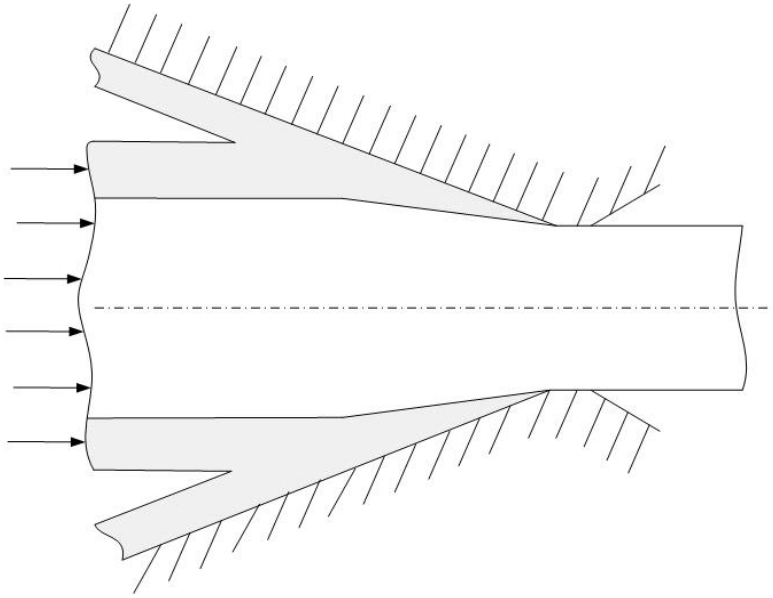

Fig. 6 Adhesive failure of polymer coating during composite rod extrusion

1.4 Research objective

To the author's best knowledge there has been no previous work done in predicting the range of process parameters for successful axisymmetric extrusion of a polymer coated metal rod. The objective of this research study is to develop an analytical model to predict success or failure of axisymmetric extrusion of polymer coated metal rod through a conical die. Although empirical optimization of the process is possible but it involves trial and error which is too tedious, expensive and time consuming and hence developing an analytical solution is more viable solution and it also enhances the understanding of the process in a better manner. An analytical model allows for optimizing the process parameters that will increase tool life, minimize power requirement and improve part quality in a cost effective manner. A commercial finite element package, ABAQUS, is used to simulate the axisymmetric extrusion using an elastic-plastic material model and validate the results predicted by the analytical model developed in this study. Initially to verify the setup of the problem, FEA simulations of simple metal rod extrusion are validated against the published theoretical results for simple metal rod extrusion. Once the finite element analysis results are compared with that of mathematical model, a range of process parameters will be evaluated to predict successful extrusion of polymer coating on the final product. An important concern in metal forming processes is whether the desired deformation can be accomplished without fracture or defects in the workpiece. Hence, an effort is made in this study to predict the failure of polymer coating during the extrusion.

CHAPTER II

LITERATURE REVIEW

The primary concern in metal forming operations is to predict the forces required to definitely cause plastic flow. Accurate prediction is difficult due to uncertainties such as frictional forces, non-homogeneous deformation and strain hardening of material during complex deformations. Hence, many researchers have developed analytical models viz. upper bound method, slip line method and slab method, to predict approximate forces required during extrusion. The upper bound method, slip line method and slab method are described concisely in Hosford et. al. [6]. As computing resources became more powerful and easily available, researchers also predicted the forces required during extrusion using the finite element method. For axisymmetric extrusion, the upper bound method is most suitable, since the slab method is more appropriate for plane strain problems, the slip line method being more complex and finite element method is too time consuming, problem specific and computing intensive. Hence it was decided that the upper bound method would be the most suitable method to develop a mathematical model for polymer coated metal rod extrusion through conical die.

Among various methods of solutions, the upper bound method as an analytical method for analysis of the axisymmetric extrusion process was first used by Kudo [9] and Avitzur [10] and has been used widely since then. Kobayashi et. al. [11] devised a method for finding kinematically admissible velocity field and stress field for

axisymmetric forming problems to find the upper and lower bound limit for axisymmetric extrusion along with two other forming operations. Bianchi et. al. [12] compared viscoplastic finite element model with slip line and upper bound method solutions for non hardening material subject to plain strain as well as axisymmetric extrusion. Even though the finite element method gives detailed information, it takes considerable computation time and thus is not yet so practical for optimizing the process in extrusion. Avitzur [5] developed condition for center bursting during extrusion and wire drawing by assuming spherical velocity field and using upper bound method for conical die. Zimmerman et. al. [13] modified their spherical velocity field by introducing additional parameter and was able to calculate lower upper bound for conical die than predicted by spherical velocity field used by Avitzur [5]. Chen et. al. [14] developed a generalized method to find velocity field from stream functions for first time and applied to three axisymmetric dies viz. cosine, elliptical and hyperbolic. Before streamline approach was developed there was no method to develop generalized velocity field and so it was just assumed to be spherical, triangular or some mathematically less intensive shaped velocity field. Velocity field derived from streamline functions give lower upper bound than spherical velocity field used by Avitzur [5]. Hence the velocity field derived from the flow functions was decided to be used to implement the upper bound method.

Chang et. al. [15] developed velocity field for axisymmetric extrusion through curved dies using upper bound method. Nagpal [16] proposed the generalized flow functions method for finding kinematically admissible velocity field for axisymmetric extrusion.

Yang et. al. [17,18] used generalized deformation boundaries and generalized velocity field using streamline flow method for analysis of axisymmetric extrusion through arbitrarily curved dies which gave lower extrusion pressure estimates than Chang et. al. [15]. He also showed that deformation boundaries are curved inside on both the ends of die and not vertical as was used by others until then. Hence curved rigid-plastic deformation boundaries would be used to develop the mathematical model as it gives lower upper bound solutions. Altan et. al. [19] proposed two different flow models and compared both of them with Avitzur's [10] spherical velocity model and found that flow function models do give lower upper bound results. Alexandrov et. al. [20] formulated kinematically admissible velocity field based on simple radial flow field combined with asymptotic behavior near velocity discontinuity to reduce complexity of mathematics involved giving nearly same results.

As it can be seen that upper bound method was almost becoming standard method to apply to axisymmetric extrusion problem and many researchers were trying to lower the upper bound solutions by developing newer methods to derive kinematically admissible velocity field. Also it was proved by and large that flow functions method to derive velocity field along with curved rigid-plastic deformation boundaries (Figure 7) give lower upper bound than spherical velocity field (Figure 8) and other methods. Hence it was decided to develop the analytical model for composite rod extrusion using upper bound method using flow function method to derive kinematically admissible velocity field with curved rigid-plastic deformation boundaries.

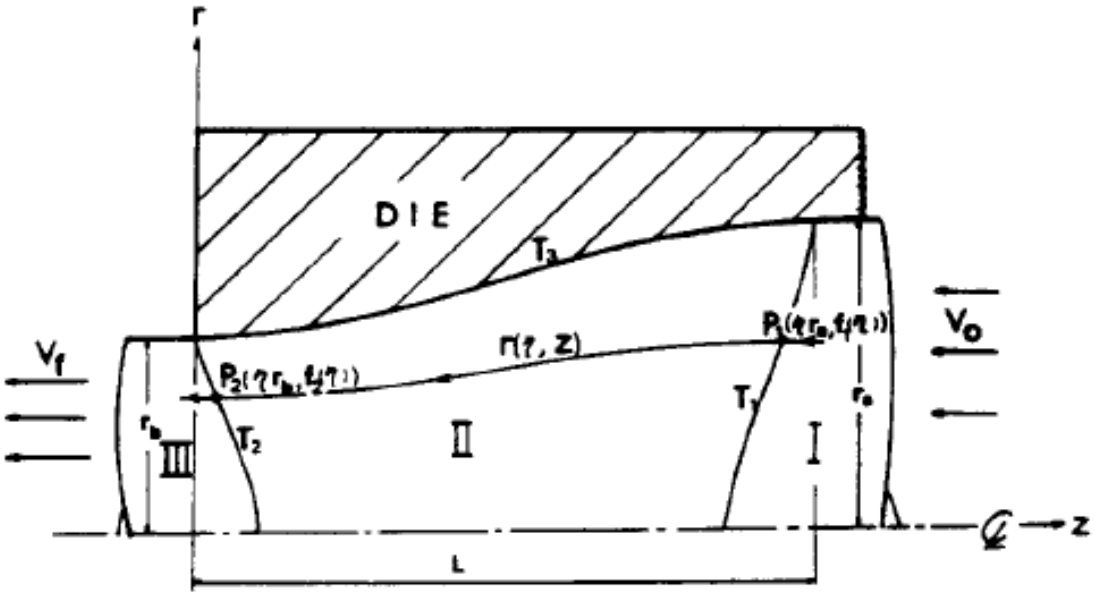

Fig. 7 General kinematically admissible velocity field derived from streamlined flow function [17]

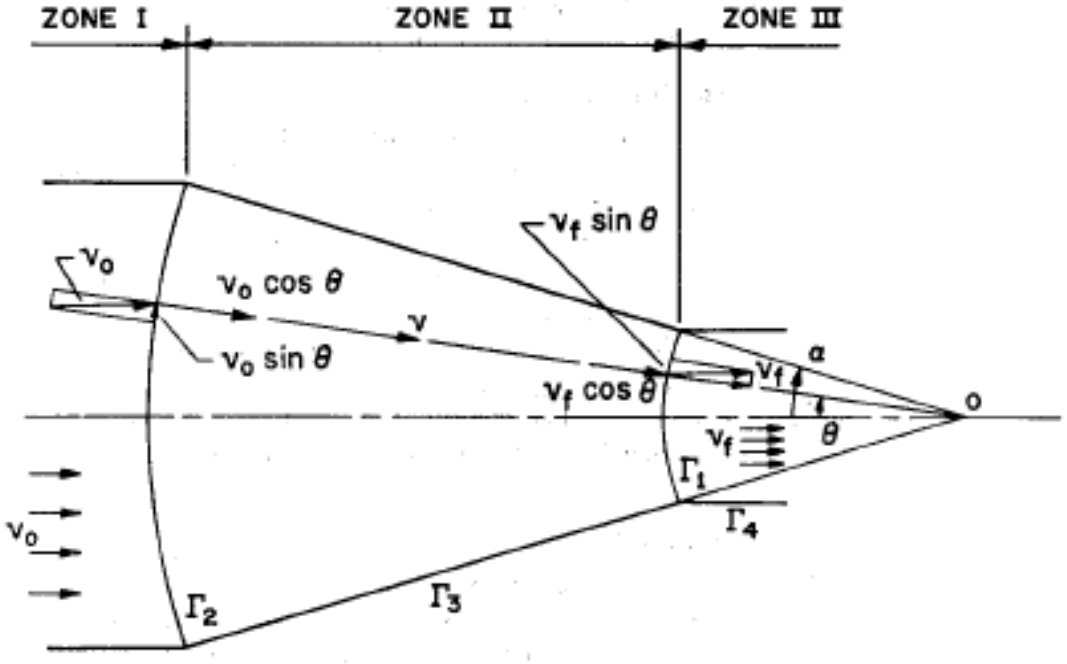

Fig. 8 Kinematically admissible spherical velocity field [10]

With advancement in technology composites had more and more applications and researchers felt need to study behavior of composites undergoing axisymmetric extrusion. But as stated earlier to best knowledge of author no study has been carried to study polymer coated metal extrusion but many researchers did studied bimetal extrusion i.e. one metal coated with another and extruded simultaneously. Osakada et. al. [21] was the first to show that composite rods can undergo successful deformation under certain process conditions. Tayal et. al. [22] suggested a finite element solution for problem of mutilayer composite extrusion which is independent of number of constituent metals involved and die geometry. Treating the flow of metals as flow of viscous, non-Newtonian incompressible fluid he even predicted the geometry of the interface separating the two materials. Avitzur et. al. [23,24] used torroidal velocity field to predict fracture of core metal in bimetallic rods during co-drawing as well as co-extrusion and hence established a fracture criterion. As it can be seen the problem was tackled by various approaches and during the course of time better and better solutions were being developed.

Yang et. al. [25] analyzed extrusion of composite rods through curved dies by using flow function approach. Two different flow functions of second order and third order are used and compared with each other. He proved that second order flow function was in better agreement with experimental observation than third order flow function in terms of predicting extrusion load and in deformation region. Hwang et. al. [26] proposed different set of initial flow function to investigate plastic deformation behavior of the

rods during axisymmetric extrusion of composite rods. Relative slip is allowed at interface of two metals. Later Kwon et. al. [27] worked on predicting the cohesive failure of the coated material using fracture criteria developed by Cockcroft et. al. [7].

And hence it is deduced that going for higher order flow functions just increases the complexity in calculations without improving the accuracy of results. So the mathematical model for polymer coated metal rod extrusion is developed by using the most basic first order flow function as it reduces the complexities. Also the rigid-plastic deformation boundaries used in developing the model would be a polynomial curve. The nature of the deformation boundary will be decided by optimization process and hence it can be curved inwards or outwards at each die end or straight as determined by the optimization. Developing a failure model of the polymer coated metal rod extrusion is very important as it gives us the working range of process parameters. Hence it was decided that failure model has to be developed which hasn't been developed by other researchers.

CHAPTER III

ANALYTICAL MODEL

This chapter presents an analytical model of polymer coated metal rod extrusion through conical die to predict range of process parameters where the extrusion would be successful. As stated earlier, finite element analysis method and experimental method, both are expensive, time consuming and impractical to optimize the problem. Hence effort is made in this study to develop a generalized analytical model, which will provide insight into the mechanism governing polymer coated metal rod extrusion and let us explore effects of various parameters on the process. Also added advantage of developing analytical model is it can predict range of process parameters of coating failure.

3.1 Upper bound method

For many plastic deformation processes, including axisymmetric extrusion, exact analytical solutions are difficult to obtain due to the mathematical complexity involved and hence researchers inevitably use some approximation method. There are many approximate but highly developed methods applied to axisymmetric extrusion, like limit analysis, slab method, slip line method and upper bound method. But among all approximate methods, upper bound method is most powerful [27] and it has been widely used to develop analytical model for numerous metal forming processes, such as forging,

wire drawing, tube sinking, strip rolling, and extrusion. The upper bound method has been used for analysis of axisymmetric rod extrusion process because of its effectiveness to optimize process parameters, design die shapes with reduced computation time.

An upper bound analysis, as the name suggests, predicts a load that will surely cause the plastic deformation of the workpiece. Unlike an exact solution, upper bound analysis doesn't need to satisfy stress equilibrium and only satisfies self consistent flow field. The upper bound analysis makes use of energy principle to equate the internal rate of energy dissipation with rate of external work done. A brief and excellent explanation about upper bound analysis is given in Hosford et. al. [8]. To apply upper bound method to polymer coated metal rod extrusion, a kinematically admissible velocity field needs to be assumed. The basic requirements for the velocity components to be kinematically admissible velocity field are given below:

- It should satisfy the incompressibility condition throughout the volume
- It should satisfy boundary conditions that allows velocity discontinuity tangential to the boundary but not normal to the boundary.

Hence the geometrical configuration of the material determines some boundary conditions and must be known. During axisymmetric extrusion the geometrical configuration of work material is confined by die surface on the outer surface and its nature at the entry and exit surface of plastic deformation is to be determined, for which there are two commonly used approaches. First one is to assume the nature of plastic

deformation boundary at entry and exit end of die such as the spherical velocity field developed by Avitzur [10] and second is to construct a velocity field by assuming proper flow functions. As discussed earlier flow functions method is employed in developing this analytical model as it gives lower upper bound and it has been shown that spherical velocity field is a special case of flow function method. Strain rates can be derived from velocity field, which can be integrated to calculate the power consumed internally in the deformation field using the appropriate strength properties of the material. In applying the upper bound technique and developing analytical model for polymer coated metal rod extrusion, several simplifying assumptions are made in this thesis and are summarized below:

- The work materials i.e. metal and polymer are isotropic and homogeneous.
- The work materials are incompressible and die is assumed to be rigid body. Usually extrusion dies are made from heat treated and hardened tool steel which has much higher yield strength than the workpiece and hence it is safe to assume the die as rigid body.
- Both metal and polymer undergo plastic deformation predominantly and elastic strain is neglected.
- Effect of temperature between the composite rod and die is neglected and the process is assumed to be isothermal because practically the extrusion die is kept cool by circulating water around it.
- A constant friction factor model is assumed for die and workpiece interface.

- Polymer and metal are symmetric about the central axis and there is no axis shift during or after the deformation.
- Coating thickness is small as compared to the metal rod radius ($t_p \leq \frac{R_m}{20}$ approx.)
- All plastic deformation occurs by shear on few discrete planes in the deformation zone. Everywhere outside the deformation zone material is considered to be rigid. Hence both metal and polymer are considered to be rigid – plastic, strain rate independent and von-Mises materials.
- For polymers phenomenon of creep is neglected and their behavior is assumed to be analogous to metals.

3.2 Upper bound model for successful extrusion of polymer coated metal rod

As discussed above polymer coated metal rod extrusion could lead to successful extrusion or one of the various failure discussed above. Both the successful and failure conditions are modeled separately in this study. Figure 9 shows generalized kinematically admissible velocity field for the mathematical model developed along with rigid-plastic boundaries marking the deformation zone. Due to symmetry about central axis it is only necessary to consider the field in any one plane containing the axis.

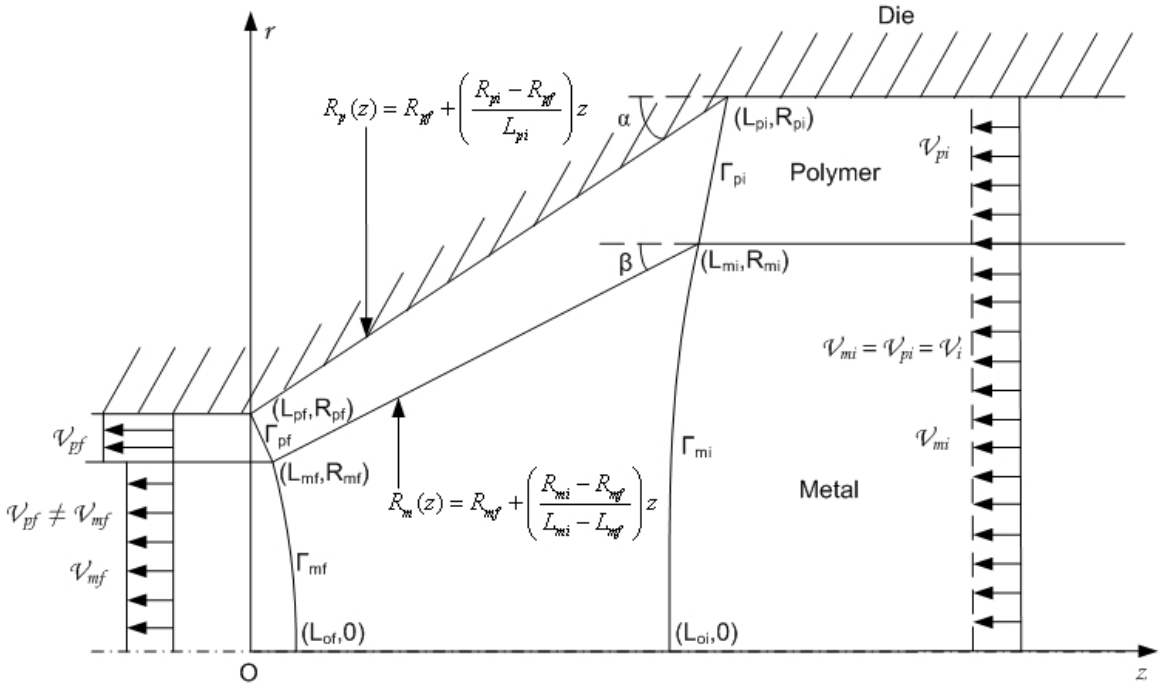

Fig. 9 Model for successful extrusion of polymer coated metal rod

3.2.1 Flow functions

(Note – Throughout the mathematical model subscript ‘m’ and ‘p’ refers to metal and polymer respectively and ‘i’ and ‘f’ refers to initial and final condition respectively. Also ‘r’ and ‘z’ refers to the respective coordinate axis wherever applicable.)

As shown by Nagpal [16] stream function for selecting generalized velocity field for axisymmetric extrusion is given as

$$\phi = f(\eta)\sum_{j=1}^{N} a_j \eta^j \tag{1}$$

where streamline constants in metal and polymer are of the form

$$\eta_m = \frac{r^2}{R_m^2(z)} \tag{2}$$

$$\eta_p = \frac{r^2 - R_m^2(z)}{R_p^2(z) - R_m^2(z)} \tag{3}$$

As discussed before in literature review going for higher order flow functions increases the complexity and does not gives any better solution and hence first order flow functions are taken in this study. Hence the flow functions for metal and polymer are given respectively

$$\begin{aligned} \phi_m &= a_{1m}\eta_m \\ \phi_p &= a_{1p}\eta_p \end{aligned} \tag{4}$$

Therefore substituting (2) and (3) in (4) we get flow functions for metal and polymer

$$\phi_m = a_{1m}\left(\frac{r^2}{R_m^2(z)}\right) \tag{5}$$

$$\phi_p = a_{1p}\left(\frac{r^2 - R_m^2(z)}{R_p^2(z) - R_m^2(z)}\right) \tag{6}$$

As rigid – perfectly plastic model is used for work material in this study the flow functions for metal and polymers have to satisfy the following boundary conditions at rigid – plastic deformation boundaries

$$\phi_m = \frac{-V_i r^2}{2} \qquad \text{on } \Gamma_{mi} \tag{7}$$

$$\phi_m = \frac{-V_{mf} r^2}{2} \qquad \text{on } \Gamma_{mf} \tag{8}$$

$$\phi_p = -V_i\left(\frac{r^2 - R_{mi}^2}{2}\right) \quad \text{on } \Gamma_{pi} \tag{9}$$

$$\phi_p = -V_{pf}\left(\frac{r^2 - R_{mf}^2}{2}\right) \quad \text{on } \Gamma_{pf} \tag{10}$$

Negative sign is due to the fact that flow from input to output die condition is in negative Z direction. Other boundary conditions to be satisfied are deduced from the geometrical configuration of the extrusion process and are given below

$$\phi_m = a_{1m} \qquad \text{at } r = R_m(z) \tag{11}$$

$$\phi_m = 0 \qquad \text{at } r = 0 \tag{12}$$

$$\phi_p = a_{1p} \qquad \text{at } r = R_p(z) \tag{13}$$

$$\phi_p = 0 \qquad \text{at } r = R_m(z) \tag{14}$$

Die function and interface function are derived from geometry and are given as

$$R_p(z) = R_{pf} + \frac{\left(R_{pi} - R_{pf}\right)}{L_{pi}} z \tag{15}$$

$$R_m(z) = R_{mf} + \left(\frac{R_{mi} - R_{mf}}{L_{mi} - L_{mf}}\right) z \tag{16}$$

By applying boundary conditions (7) and (11), a_{1m} can be solved as

$$\phi_m = \frac{-V_i R_m^2\left(L_{mi}\right)}{2} = a_{1m}\left(\frac{R_m^2(z)}{R_m^2(z)}\right)$$

$$a_{1m} = \frac{-V_i R_m^2}{2} \tag{17}$$

Similarly by applying boundary conditions (9) and (13) a_{1p} can be solved as

$$\phi_p = -V_i \frac{\left(R_p^2(L_{mi}) - R_{mi}^2\right)}{2} = a_{1p}\left(\frac{R_p^2(z) - R_m^2(z)}{R_p^2(z) - R_m^2(z)}\right)$$

$$a_{1p} = \frac{-V_i\left(R_{pi}^2 - R_{mi}^2\right)}{2} \tag{18}$$

Substituting (17) in (5) flow function for streamlines in metal is given

$$\phi_m = \frac{-V_i R_{mi}^2}{2}\left(\frac{r^2}{R_m^2(z)}\right) \tag{19}$$

Similarly substituting (18) in (6) flow function for streamline in polymer is given

$$\phi_p = \frac{-V_i\left(R_{pi}^2 - R_{mi}^2\right)}{2}\left(\frac{r^2 - R_m^2(z)}{R_p^2(z) - R_m^2(z)}\right) \tag{20}$$

Boundary conditions given by (8) and (10) are satisfied automatically by the virtue of mass flow rate remains equal

$$V_i R_{mi}^2 = V_{mf} R_{mf}^2 \tag{21}$$

$$V_i\left(R_{pi}^2 - R_{mi}^2\right) = V_{pf}\left(R_{pf}^2 - R_{mf}^2\right) \tag{22}$$

Also boundary conditions given by (12) and (14) are satisfied due to proper choice of η

3.2.2 Rigid-plastic deformation boundary

Researchers using flow function method to derive kinematically admissible velocity field have mostly used mostly straight rigid-plastic boundary which is fixed. Rigid-plastic deformation boundary is modeled as a polynomial curve to lower the upper

bound result. At the same time the rigid-plastic deformation boundary is kept flexible by allowing the optimization method to determine the exact nature of curve.

Deformation boundary in the polymer is assumed to have a linear relationship because the thickness of polymer coating is very small as compared to the core metal and hence the contribution of shear losses at those boundaries is small as compared to the total power required. Equation governing rigid plastic boundaries in polymer is given as

Let $\Gamma_{pf} = a + bz$ (23)

Solving for a and b by applying boundary conditions at die and metal-polymer interface

at $r = R_{pf}$ and $z = 0 \Rightarrow a = R_{pf}$ (24)

at $r = R_{mf}$ and $z = L_{mf} \Rightarrow \mathrm{b} = \dfrac{R_{mf} - R_{pf}}{L_{mf}}$ (25)

Substituting (24) and (25) in (23) final equation for rigid-plastic boundary in polymer material at exit of die is given as

$$\Gamma_{pf} = R_{pf} + \left(\frac{R_{mf} - R_{pf}}{L_{mf}} \right) z \tag{26}$$

Applying the similar approach for the rigid-plastic boundary in polymer material at entry of die equation for Γ_{pi} can be derived. Boundary conditions at entry of die are

at $r = R_{pi}$ and $z = L_{pi}$ (27)

at $r = R_{mi}$ and $z = L_{mi}$ (28)

Substituting (27) and (28) in (23) final equation for rigid-plastic boundary in polymer material at entry of die is given as

$$\Gamma_{pi} = \left(\frac{R_{mi} L_{pi} - R_{pi} L_{mi}}{L_{pi} - L_{mi}} \right) + \left(\frac{R_{pi} - R_{mi}}{L_{pi} - L_{mi}} \right) z \tag{29}$$

Rigid-plastic deformation boundary in metal at die exit is assumed to be second order polynomial and its general equation is given as

$$\text{Let } \Gamma_{mf} \Rightarrow z = ar^2 + br + c \tag{30}$$

Applying Boundary condition due to axis of symmetry and solving for constant

$$\text{at } r = 0 \text{ and } z = L_{of} \Rightarrow \text{c} = L_{of} \tag{31}$$

Due to axisymmetric extrusion the rigid-plastic deformation surface has to be perpendicular to the axis of symmetry or else there will be singularity. Hence applying that boundary condition and solving for constant

$$\left. \frac{dz}{dr} \right|_{r=0} = 0 \Rightarrow 2ar + b = 0 \Rightarrow b = 0 \tag{32}$$

Also boundary condition due to metal polymer interface needs to be satisfied

$$\text{at } r = R_{mf} \text{ and } z = L_{mf} \Rightarrow a = \frac{L_{mf} - L_{of}}{R_{mf}^2} \tag{33}$$

Substituting the values of constant derived in (31), (32) and (33) in (30) general equation for rigid-plastic deformation boundary at exit of die in metal, Γ_{mf} is given as

$$z = \left(\frac{L_{mf} - L_{of}}{R_{mf}^2} \right) r^2 + L_{of}$$

$$\Gamma_{mf} \Rightarrow r = \sqrt{\frac{(z - L_{of})R_{mf}^2}{(L_{mf} - L_{of})}} \tag{34}$$

Similarly assuming rigid-plastic deformation boundary in metal at die entry as given in (30) and applying boundary conditions

$$\text{at } r = 0 \text{ and } z = L_{oi} \tag{35}$$

$$\text{at } r = R_{mi} \text{ and } z = L_{mi} \tag{36}$$

$$\left.\frac{dz}{dr}\right|_{r=0} = 0 \tag{37}$$

Substituting (35), (36) and (37) in (30) and solving for constants we get the final form of equation of rigid-plastic deformation boundary for metal at die entry as

$$\Gamma_{mi} \Rightarrow r = \sqrt{\frac{(z - L_{oi})R_{mf}^2}{(L_{mf} - L_{oi})}} \tag{38}$$

Hence the equations of rigid-plastic deformation boundary can be summarized as below

$$\Gamma_{pf} = R_{pf} + \left(\frac{R_{mf} - R_{pf}}{L_{mf}}\right)z \tag{26}$$

$$\Gamma_{pi} = \left(\frac{R_{mi}L_{pi} - R_{pi}L_{mi}}{L_{pi} - L_{mi}}\right) + \left(\frac{R_{pi} - R_{mi}}{L_{pi} - L_{mi}}\right)z \tag{29}$$

$$\Gamma_{mf} \Rightarrow r = \sqrt{\frac{(z - L_{of})R_{mf}^2}{(L_{mf} - L_{of})}} \tag{34}$$

$$\Gamma_{mi} \Rightarrow r = \sqrt{\frac{(z - L_{oi})R_{mf}^2}{(L_{mf} - L_{oi})}} \tag{38}$$

3.2.3 Velocity field

In zone II, V_r and V_z are velocities in r and z directions respectively and can be determined from flow functions as

$$V_r = -\frac{1}{r}\frac{\partial \phi}{\partial z} \tag{39}$$

$$V_z = \frac{1}{r}\frac{\partial \phi}{\partial r} \tag{40}$$

Using (39) and (40) to find velocity in metal in r and z direction respectively as given

$$V_{rm} = -\frac{1}{r}\frac{\partial \phi_m}{\partial z} = -V_i R_{mi}^2 \left(\frac{r R_m'(z)}{R_m^3(z)} \right) \tag{41}$$

$$V_{zm} = \frac{1}{r}\frac{\partial \phi_m}{\partial r} = -\frac{V_i R_{mi}^2}{R_m^2(z)} \tag{42}$$

Similarly using (39) and (40) velocity in polymer in r and z direction is given as

$$V_{rp} = -\frac{1}{r}\frac{\partial \phi_p}{\partial z} = -\frac{V_i\left(R_{pi}^2 - R_{mi}^2\right)}{r}\left[\frac{R_m(z)R_m'(z)(R_p^2(z) - r^2) + R_p(z)R_p'(z)(r^2 - R_m^2(z))}{(R_p^2(z) - R_m^2(z))^2} \right] \tag{43}$$

$$V_{zp} = \frac{1}{r}\frac{\partial \phi_p}{\partial r} = -V_i\left(\frac{R_{pi}^2 - R_{mi}^2}{R_p^2(z) - R_m^2(z)} \right) \tag{44}$$

where,

$$R_m'(z) = \frac{dR_m(z)}{dz} \tag{45}$$

$$R_p'(z) = \frac{dR_p(z)}{dz} \tag{46}$$

Note that

$$\left.\frac{V_{rm}}{V_{zm}}\right|_{r=R_m(z)} = R_m'(z) \quad \text{and} \tag{47}$$

$$\left.\frac{V_{rp}}{V_{zp}}\right|_{r=R_p(z)} = R_p'(z) \tag{48}$$

This proves that velocity field derived follows the die profile and interface profile and hence satisfies the geometrical boundary conditions at the surface. Hence this velocity field derived from the flow functions assumed satisfies one of the conditions to be kinematically admissible.

3.2.4 Velocity discontinuity

Velocity discontinuity is the tangential velocity along any rigid-plastic deformation boundary that a particle suffers when it crosses that boundary. These discontinuities are the reason for shear losses across these boundaries and hence add up to the total internal energy dissipation. $(\Delta V)_\Gamma$ is the difference between velocity component tangential to boundary given by Γ. Hence velocity discontinuity at Γ_{mi} is given as

$$\left|\Delta V_i\right|_{\Gamma_{mi}} = \left|\left(V_i + V_{zm}\right)\frac{dz}{ds} - V_{rm}\frac{dr}{ds}\right| \tag{49}$$

This can be rearranged as following

$$\left|\Delta V_i\right|_{\Gamma_{mi}} = \left|\left(V_i + V_{zm}\right) - V_{rm}\frac{dr}{dz}\right|\frac{dz}{ds} \tag{50}$$

Similarly Velocity discontinuity at Γ_{pi} is given as

$$\left|\Delta V_i\right|_{\Gamma_{pi}} = \left|\left(V_i + V_{zp}\right)\frac{dz}{ds} - V_{rp}\frac{dr}{ds}\right|$$

which can be rearranged as,

$$\left|\Delta V_i\right|_{\Gamma_{pi}} = \left|\left(V_i + V_{zp}\right) - V_{rp}\frac{dr}{dz}\right|\frac{dz}{ds} \tag{51}$$

Similarly velocity discontinuity at Γ_{mf} is given as

$$\left|\Delta V_f\right|_{\Gamma_{mf}} = \left|\left(V_{mf} + V_{zm}\right) - V_{rm}\frac{dr}{dz}\right|\frac{dz}{ds} \tag{52}$$

And velocity discontinuity at Γ_{pf} is given as

$$\left|\Delta V_f\right|_{\Gamma_{pf}} = \left|\left(V_{pf} + V_{zp}\right) - V_{rp}\frac{dr}{dz}\right|\frac{dz}{ds} \tag{53}$$

Just like rigid-plastic deformation boundary there is a velocity discontinuity where ever there is interface between two materials. Hence Velocity discontinuity between die surface and polymer is given as

$$\left|\Delta V\right|_{R_p} = \left|V_{zp}\right|_{r=R_p}\left[1 + \left(R_p'(z)\right)^2\right]^{\frac{1}{2}} \tag{54}$$

And velocity discontinuity between metal and polymer is given as

$$\left|\Delta V\right|_{R_m} = \left|V_{zp} - V_{zm}\right|_{r=R_m}\left[1 + \left(R_m'(z)\right)^2\right]^{\frac{1}{2}} \tag{55}$$

3.2.5 Strain rates

Strain rates can be determined from velocity and are used to calculate effective strain rate which in turn is used to calculate total power. We know from knowledge of elasticity that strains are given by

$$\varepsilon_{ij} = \frac{1}{2}\left(U_{i,j} + U_{j,i}\right) \tag{56}$$

Hence strain rates are given by

$$\dot{\varepsilon}_{ij} = \frac{1}{2}\left(V_{i,j} + V_{j,i}\right) \tag{57}$$

Applying the above principle given by (57) strain rates in metal are derived below as

$$\begin{aligned}\dot{\varepsilon}_{rrm} &= \frac{\partial V_{rm}}{\partial r} \\ &= -\frac{V_i R_{mi}^2 R_m'(z)}{R_m^3(z)}\end{aligned} \tag{58}$$

$$\begin{aligned}\dot{\varepsilon}_{zzm} &= \frac{\partial V_{zm}}{\partial z} \\ &= \frac{2V_i R_{mi}^2 R_m'(z)}{R_m^3(z)}\end{aligned} \tag{59}$$

$$\begin{aligned}\dot{\varepsilon}_{\theta\theta m} &= \frac{V_{rm}}{r} \\ &= -\frac{V_i R_{mi}^2 R_m'(z)}{R_m^3(z)}\end{aligned} \tag{60}$$

$$\begin{aligned}\dot{\varepsilon}_{rzm} &= \frac{1}{2}\left(\frac{\partial V_{zm}}{\partial r} + \frac{\partial V_{rm}}{\partial z}\right) \\ &= -V_i R_{mi}^2 \left(\frac{r R_m''(z)}{2R_m^3(z)} - \frac{3r\left(R_m'(z)\right)^2}{2R_m^4(z)}\right)\end{aligned} \tag{61}$$

Since $V_{\theta m} = 0$

Therefore, $\varepsilon_{r\theta m} = 0$ (62)

And similarly $\varepsilon_{z\theta m} = 0$ (63)

It is important to note that $\dot{\varepsilon}_{rrm} + \dot{\varepsilon}_{zzm} + \dot{\varepsilon}_{\theta\theta m} = 0$

Sum of all the principal strains is zero which satisfies the condition of incompressibility and hence we can verify that the flow functions we have chosen are valid flow functions for flow in metal through conical die. Hence the velocity field derived from the flow functions satisfies another important criterion to be kinematically admissible velocity field, which is a primary requirement for upper bound method to be applicable.

Applying the above principle given by (57) strain rates in polymer are derived below as

$$\dot{\varepsilon}_{rrp} = \frac{\partial V_{rp}}{\partial r} = -V_i\left(R_{pi}^2 - R_{mi}^2\right)\left[\frac{R_p(z)R_p'(z)\left(r^2 + R_m^2(z)\right) - R_m(z)R_m'(z)\left(r^2 + R_p^2(z)\right)}{r^2\left(R_p^2(z) - R_m^2(z)\right)^2}\right] \quad (64)$$

$$\dot{\varepsilon}_{zzp} = \frac{\partial V_{zp}}{\partial z} = 2V_i\left(R_{pi}^2 - R_{mi}^2\right)\left[\frac{R_p(z)R_p'(z) - R_m(z)R_m'(z)}{\left(R_p^2(z) - R_m^2(z)\right)^2}\right] \quad (65)$$

$$\dot{\varepsilon}_{\theta\theta p} = \frac{V_{rp}}{r} = -V_i\left(R_{pi}^2 - R_{mi}^2\right)\left[\frac{R_m(z)R_m'(z)\left(R_p^2(z) - r^2\right) + R_p(z)R_p'(z)\left(r^2 - R_m^2(z)\right)}{r^2\left(R_p^2(z) - R_m^2(z)\right)^2}\right] \quad (66)$$

$$\dot{\varepsilon}_{rzp} = \frac{1}{2}\left(\frac{\partial V_{zp}}{\partial r} + \frac{\partial V_{rp}}{\partial z}\right)$$
$$= -\frac{V_i\left(R_{pi}^2 - R_{mi}^2\right)}{2r}\left[\frac{\mathrm{R'^2_m(z)\left(R^2_p(z) - r^2\right) + R'^2_p(z)\left(r^2 - R^2_m(z)\right)}}{\left(\mathrm{R^2_p(z) - R^2_m(z)}\right)^2} - \right.$$
$$\left.\frac{4\left(R_p(z)R'_p(z) - R_m(z)R'_m(z)\right)\left(R_m(z)R'_m(z)\left(R_p^2(z) - r^2\right) + R_p(z)R'_p(z)\left(r^2 - R_m^2(z)\right)\right)}{\left(R_p^2(z) - R_m^2(z)\right)^3}\right] \quad (67)$$

Since $V_{\theta p} = 0$

Therefore, $\varepsilon_{r\theta p} = 0$ (68)

And $\varepsilon_{z\theta p} = 0$ (69)

Again note that $\dot{\varepsilon}_{rrp} + \dot{\varepsilon}_{zzp} + \dot{\varepsilon}_{\theta\theta p} = 0$

Sum of all the principal strains is zero which satisfies the condition of incompressibility and hence we can deduce that we have chosen a valid flow function for flow in polymer.

3.2.6 Total power

As the name suggest the power predicted by upper bound theorem is always greater than the actual power required for carrying out the axisymmetric extrusion. According to the upper bound theorem total power dissipated is given as sum of the power required for internal deformation, friction losses and shear losses and is given by this simple equation

$$J^* = \dot{W}_i + \dot{W}_f + \dot{W}_s \quad (70)$$

where,

$\dot{W}_i$ = total internal power required for deformation

$\dot{W}_s$ = total power of shear deformation

$\dot{W}_f$ = total frictional power dissipated

3.2.6.1 Power for internal deformation

Rate of energy dissipation for internal deformation is given by

$$\dot{W}_i = \int \bar{\sigma}\dot{\bar{\varepsilon}} dV \tag{71}$$

The constitutive law of rigid-plastic material yielding by von-Mises criterion gives effective stress and strain rate as

$$\bar{\sigma} = \sigma_0 \tag{72}$$

$$\dot{\bar{\varepsilon}} = \frac{2}{3}\sqrt{\frac{1}{2}\dot{\varepsilon}_{ij}\dot{\varepsilon}_{ij}} \tag{73}$$

Total internal power dissipated for plastic deformation is sum of two parts; first power required for plastic deformation of metal and second power required for plastic deformation of polymer and is given as

$$\dot{W}_i = \left(\dot{W}_i\right)_m + \left(\dot{W}_i\right)_p$$

$$\dot{W}_i = \frac{2}{3}\left(\sigma_0\right)_m\left[\int_V \sqrt{\frac{1}{2}\dot{\varepsilon}_{ij}\dot{\varepsilon}_{ij}}\, dV\right] + \frac{2}{3}\left(\sigma_0\right)_p\left[\int_V \sqrt{\frac{1}{2}\dot{\varepsilon}_{ij}\dot{\varepsilon}_{ij}}\, dV\right] \tag{74}$$

which can be expanded as

$$\dot{W}_i = \frac{2}{\sqrt{3}}(\sigma_0)_m \left[\int_0^{2\pi} \int_{L_{of}}^{L_{oi}} \int_0^{R_m(z)} \sqrt{\frac{1}{2}\left(\dot{\varepsilon}_{ij}\right)_m \left(\dot{\varepsilon}_{ij}\right)_m}\, r d\theta dr dz + \int_0^{2\pi} \int_{L_{mf}}^{L_{of}} \int_{\Gamma_{mf}}^{R_m(z)} \sqrt{\frac{1}{2}\left(\dot{\varepsilon}_{ij}\right)_m \left(\dot{\varepsilon}_{ij}\right)_m}\, r d\theta dr dz + \int_0^{2\pi} \int_{L_{oi}}^{L_{mi}} \int_{\Gamma_{mi}}^{R_m(z)} \sqrt{\frac{1}{2}\left(\dot{\varepsilon}_{ij}\right)_m \left(\dot{\varepsilon}_{ij}\right)_m}\, r d\theta dr dz \right] + \frac{2}{\sqrt{3}}(\sigma_0)_p \left[\int_0^{2\pi} \int_{L_{mf}}^{L_{mi}} \int_{R_m(z)}^{R_p(z)} \sqrt{\frac{1}{2}\left(\dot{\varepsilon}_{ij}\right)_p \left(\dot{\varepsilon}_{ij}\right)_p}\, r d\theta dr dz + \int_0^{2\pi} \int_0^{L_{mf}} \int_{\Gamma_{pf}}^{R_p(z)} \sqrt{\frac{1}{2}\left(\dot{\varepsilon}_{ij}\right)_p \left(\dot{\varepsilon}_{ij}\right)_p}\, r d\theta dr dz + \int_0^{2\pi} \int_{L_{mi}}^{L_{pi}} \int_{\Gamma_{pi}}^{R_p(z)} \sqrt{\frac{1}{2}\left(\dot{\varepsilon}_{ij}\right)_p \left(\dot{\varepsilon}_{ij}\right)_p}\, r d\theta dr dz \right] \tag{75}$$

Strain rate $\dot{\varepsilon}$ in metal can be derived as given below

$$\begin{aligned} \dot{\varepsilon}_m &= \sqrt{\frac{1}{2}\left(\dot{\varepsilon}_{ij}\right)_m \left(\dot{\varepsilon}_{ij}\right)_m} \\ &= \sqrt{\frac{1}{2}\left(\dot{\varepsilon}_{rrm}^2 + \dot{\varepsilon}_{zzm}^2 + \dot{\varepsilon}_{\theta\theta m}^2 + 2\dot{\varepsilon}_{rzm}^2 + 2\dot{\varepsilon}_{r\theta m}^2 + 2\dot{\varepsilon}_{z\theta m}^2\right)} \end{aligned} \tag{76}$$

Since, $\dot{\varepsilon}_{r\theta m} = 0$ and $\dot{\varepsilon}_{z\theta m} = 0$

Substituting (61) and (62) in (76) we get

$$\dot{\varepsilon}_m = \sqrt{\frac{1}{2}\left(\dot{\varepsilon}_{rrm}^2 + \dot{\varepsilon}_{zzm}^2 + \dot{\varepsilon}_{\theta\theta m}^2 + 2\dot{\varepsilon}_{rzm}^2\right)} \tag{77}$$

Substituting (57), (58), (59) and (60) in (79) and simplifying we get

$$\dot{\varepsilon}_m = \sqrt{\frac{3V_i^2 R_{mi}^4 R_m'^2(z)}{R_m^6(z)} + \frac{9V_i^2 R_{mi}^2 r^2 R_m'^2(z)}{4R_m^8(z)}} \tag{78}$$

Similarly strain rate in polymer can be derived,

$$\dot{\varepsilon}_p = \sqrt{\frac{1}{2}\left(\dot{\varepsilon}_{rrp}^2 + \dot{\varepsilon}_{zzp}^2 + \dot{\varepsilon}_{\theta\theta p}^2 + 2\dot{\varepsilon}_{rzp}^2\right)} \tag{79}$$

3.2.6.2 Power due to shear deformation

Due to tangential component of the velocity along the rigid-plastic deformation boundaries there are shear losses and power due to shear losses is given by

$$\dot{W}_s = \frac{\overline{\sigma}_0}{\sqrt{3}} \int_\Gamma \left|\Delta V\right|_\Gamma ds \tag{80}$$

The velocity field developed has four rigid-plastic deformation boundaries viz. at the entry of die in metal and polymer and at the exit end of die in metal and polymer. Consequently there is velocity discontinuity along all the four above mentioned deformation boundaries accounting for shear losses at each boundary. Hence the power required due to shear losses at the four rigid plastic deformation boundaries is sum of the power dissipated at each boundary and is given by

$$\begin{aligned}\dot{W}_s = {} & \frac{2\pi(\sigma_0)_m}{\sqrt{3}}\left(\int_{L_{oi}}^{L_{mi}} \left|\Delta V\right|_{\Gamma_{mi}} \Gamma_{mi}\sqrt{1+\Gamma_{mi}'^2}\, dz + \int_{L_{mf}}^{L_{of}} \left|\Delta V\right|_{\Gamma_{mf}} \Gamma_{mf}\sqrt{1+\Gamma_{mf}'^2}\, dz\right) + \\ & \frac{2\pi(\sigma_0)_p}{\sqrt{3}}\left(\int_{L_{mi}}^{L_{pi}} \left|\Delta V\right|_{\Gamma_{pi}} \Gamma_{pi}\sqrt{1+\Gamma_{pi}'^2}\, dz + \int_{L_{pf}}^{L_{mf}} \left|\Delta V\right|_{\Gamma_{pf}} \Gamma_{pf}\sqrt{1+\Gamma_{pf}'^2}\, dz\right)\end{aligned} \tag{81}$$

Total power dissipated due to shear losses given by equation (83) can be determined by substituting the velocity discontinuity along all the 4 rigid-plastic boundaries given by equations (50), (51), (52) and (53)

3.2.6.3 Power due to friction losses

Since there is relative motion between the work material and die surface during extrusion process there are frictional losses. Actual mechanics of friction is very complex and there are some laws are used to model friction based on common simplifying assumptions made for determining friction stress τ between the work piece and the tool. Two such laws used for modeling friction commonly are Coulomb friction law and constant friction law.

In Coulomb Friction law, friction stress τ at the contact surface is directly proportional to the contact pressure p, between the rod and the die, and is given by $\tau = \mu p$. Constant of proportionality μ is called coulomb coefficient of friction and is assumed to be constant for a particular setup. While applying Constant Friction law, friction stress τ at the contact surface is directly proportional to the flow strength of the material, σ_0, and is given by $\tau = m\sigma_0 / \sqrt{3}$. Constant of proportionality, m is called friction factor. Its value is assumed to be constant for a particular setup with $0 \le m \le 1$.

Coulomb friction law is not suitable for bulk metal forming processes like rod extrusion because it involve high contact pressures, which sometimes predicts friction stresses greater than the shear strength of the material suggesting sticking model rather than sliding model at the interface. This law is more suitable for sheet metal forming processes where contact pressures are much lower. On the other hand Constant friction

law is more suitable for bulk metal forming processes because, unlike Coulomb friction, the amount of friction is independent of the contact pressure.

Hence applying constant friction law, frictional power dissipated along the die surface and interface of metal and polymer can also be obtained from the velocity discontinuities given by (54) and (55) along these surfaces as

$$\dot{W}_f = \frac{2\pi m_m (\sigma_0)_m}{\sqrt{3}} \int_{L_{mf}}^{L_{mi}} |\Delta V|_{R_m(z)} \sqrt{1+R_m'^2(z)}\,dz + \frac{2\pi m_p (\sigma_0)_p}{\sqrt{3}} \int_0^{L_{pi}} |\Delta V|_{R_p(z)} \sqrt{1+R_p'^2(z)}\,dz \qquad (82)$$

Although in the successful extrusion bonding between polymer and metal is assumed to be perfect and there wouldn't be any friction at polymer-metal interface. This condition is imposed by keeping friction coefficient between the two materials to be zero ($m_m = 0$)

There are numerous ways to develop a kinematically admissible velocity field, hence it is important to optimize the total power with respect to geometric variables. Hence the successful axisymmetric extrusion model is optimized with respect to five geometric variables $L_{oi}, L_{of}, L_{mi}, L_{mf}$ and R_{mf} to vary the geometry of velocity field to determine minimum upper bound solution. Allowing the four length parameters to change due to optimization gives the model capability to obtain the nature of rigid-plastic boundaries by minimum power law. Also it is important to note that final coating thickness is variable and it is not assumed to be in fixed proportion of the initial thickness to initial radius.

3.3 Upper bound method for failure of polymer coating

Figure 10(a) and (b) show the shear planes for the velocity discontinuity field and hodograph, respectively, for polymer coated metal rod extrusion where polymer coating is shaved off the metal rod at the die entry. Note that plot is not to scale and polymer coating is exaggerated to show details of velocity discontinuity field and shear planes with clarity. Although this type of velocity discontinuity field is postulated for plane strain extrusion in Hosford et. al. [6] it can be applied to polymer coating because the thickness of polymer is very less as compared to its distance from axis and hence the effect of curvature is reduced greatly. Also if the polymer coating is imagined to cut open along its length and then unrolled it would appear as an infinitely wide sheet of polymer undergoing extrusion. Hence it satisfies the criteria of plane strain and this approach is practical has been proven by Jawroski et. al. [28], who applied similar approach to develop shaving model for polymer coated metal can ironing which is also an axisymmetric plastic deformation process. The difference in the velocity field developed in this study is that the final coating thickness of the shaved polymer is not assumed to be same as the initial coating thickness of the incoming work piece as used by Jawroski et. al. [28]. More complex velocity discontinuity fields may be developed to obtain still lower values of an upper bound, but this simpler field developed here is considered sufficient to demonstrate the idea of modeling failed extrusion and obtain applicable results. Also keeping the deformation field simpler reduces the mathematical complexity.

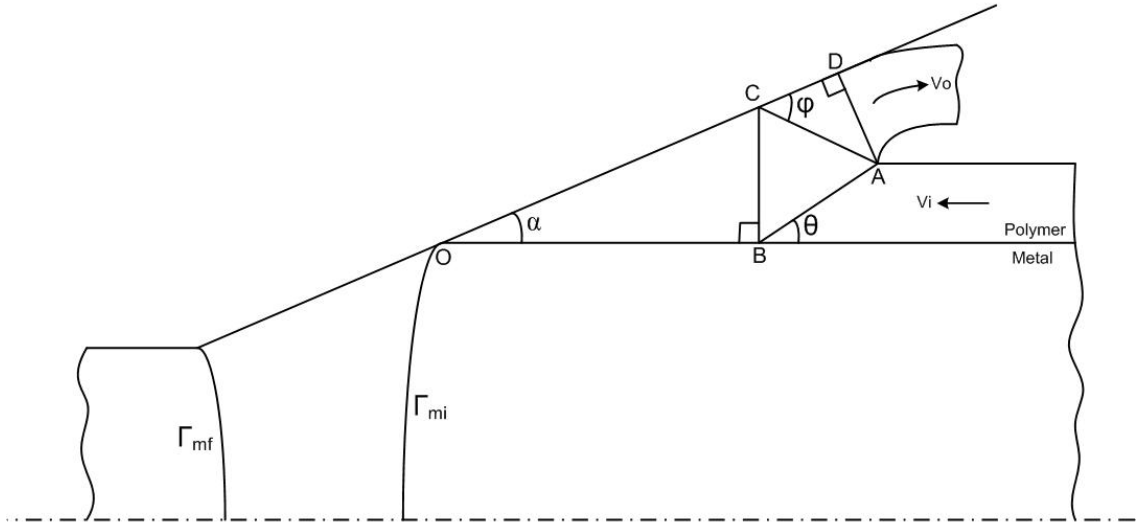

(a)

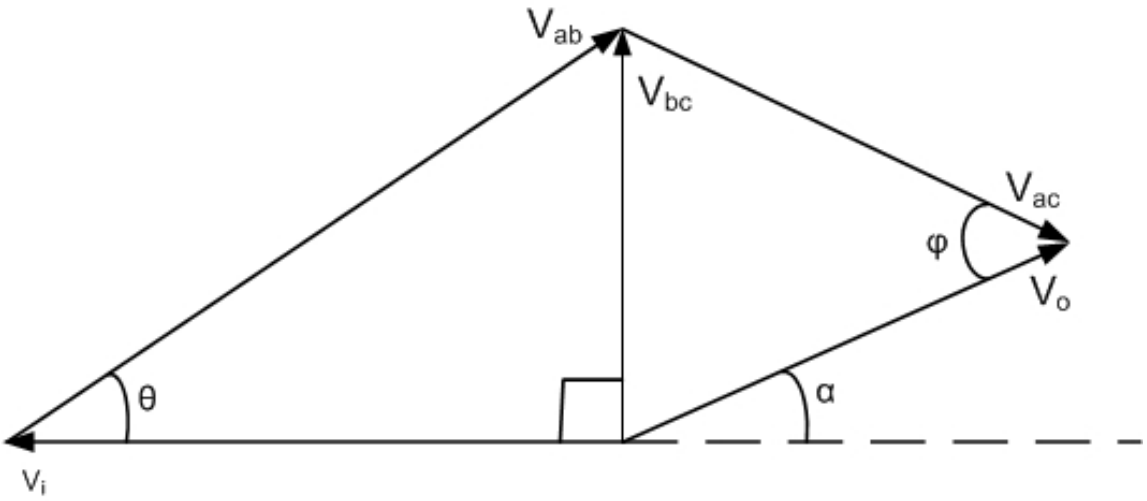

(b)

Fig. 10 Mathematical model for failure of polymer coating showing (a) velocity discontinuity field (b) and the respective hodograph

Due to polymer coating getting shaved at the die entry in this shaving model the power calculated for internal deformation, shear losses at die entry and die exit still remains the same.

Tangential velocity along the shear planes can be determined from geometry as given below

$$V_{AB} = \frac{V_i}{\cos(\theta)} \tag{83}$$

$$V_{BC} = V_i \tan(\theta) \tag{84}$$

$$V_{AC} = \frac{V_{BC} \cos(\alpha)}{\sin(\phi)} \tag{85}$$

$$V_o = \frac{V_{AC} \cos(\phi - \alpha)}{\cos(\alpha)} \tag{86}$$

It is important to note that the shaved off polymer or 'chips' do not have same exit velocity as the inlet velocity of polymer coating into the die. And hence the thickness of the chips is also not same as the initial thickness of polymer coating. Final coating thickness can be determined from mass flow principle

$$t_o = \sqrt{\frac{V_i t_i^2}{V_o}} \tag{87}$$

Friction is assumed to exist between metal and die at the metal and die interface all along the die length due to polymer coating being shaved off. Also friction is assumed to be existing between polymer and metal along length OB. There is energy dissipation at shear planes AB, BC and CA due to tangential velocity discontinuity across these planes.

The actual length of contact between the shaved off material and the tooling is difficult to predict and hence following approximation is used

$$L_{CD} = t_o \cot\phi \tag{88}$$

which is taken from solid film lubrication studies of Wilson et. al. [29]. Hence there is frictional energy dissipation along length CD due to the 'chips' in contact with die. The lengths of shear planes can be determined from geometry as given below

$$L_{AB} = \frac{t_i}{\sin(\theta)} \tag{89}$$

$$L_{AC} = \frac{t_o}{\sin(\phi)} \tag{90}$$

$$L_{BC} = t_i\left(1 + \frac{\sin(\phi - \alpha)}{\sin(\theta)}\right) \tag{91}$$

$$L_{OB} = \frac{L_{BC}}{\tan(\alpha)} \tag{92}$$

Total upper bound for polymer coating failure is sum of power given by equation (46) and power dissipated for shear losses and frictional losses given by

$$P = \sum_{shear} kAV + \sum_{friction} mkAV \tag{93}$$

As for the successful extrusion model total power for failure model is also optimized with respect to geometric parameters θ and ϕ along with L_{oi}, L_{of} and L_{mi}. This gives the optimum power required if failure as described in model were to occur. By comparing the optimized power predicted by successful extrusion model and shaving model range of process parameters can be determined which would result in successful extrusion.

3.4 Optimization of power

The power estimated by upper bound method is always greater than the actual power required for the deformation process. Hence it is necessary to minimize the power predicted by upper bound method so that it approaches the exact result. The total power required, given by Equation (70) is to be optimized with respect to all the geometric parameters. Optimization of power functional is modeled as non linear non constraint multi variable optimization and simplex search algorithm is used to carry out the optimization. The simplex search method is employed via function '*fminsearch*' in MATLAB which is also called Nelder and Mead simplex search for the algorithm it follows [30]. Numerical integration is implemented using function '*quadl*' and implements a high order method using an adaptive Gauss/Lobatto quadrature rule. The five parameters for optimization were L_{oi}, L_{of}, L_{mi}, L_{mf} and R_{mf} shown in Figure 9. Hence the nature of rigid plastic deformation boundary and final coating thickness is determined by the process of optimization. Optimization was done in two steps where in first step all the values for parameters were given in SI units or meter. In second step the optimized values of the five parameters were converted into millimeter and ran only for single iteration to give upper bound power integral. This has to be done because of the method '*quadl*' used for numerical integration. It is believed that giving the values of parameters in millimeter would make the method to take higher divisions and give better results. The MATLAB code is given in Appendix I.

Simplex method is a direct search method that does not uses numerical and analytical gradients. An N dimensional simplex is the closed geometrical entity obtained by joining N+1 point. Hence a two dimensional simplex looks like triangle and three dimensional looks like a tetrahedron. Hence sometimes simplex method is also called polyhedron search method. The guiding principle of simplex search algorithm is to find the functional at all the N+1 vertices and move the simplex away from the vertex of maximum functional value and hence towards the optimum point through a iterative process. This movement is achieved either by reflection, contraction or expansion operation. Simplex search algorithm and all the three operations described above are explained by Rao [31] and is given briefly in Appendix II.

CHAPTER IV

FINITE ELEMENT ANALYSIS

Finite element simulations are used to compare with the results of analytical model. A commercial finite element analysis (FEA) tool – ABAQUS is used to simulate the extrusion of polymer coated metal rod through conical die using elastic-plastic material model. For plastic deformation process like extrusion, FEA simulations can predict the extrusion pressure to definitely cause the extrusion with fair accuracy. But it is important to understand that FEA gives results for a particular set of tooling and process parameters and it doesn't improves the understanding of process readily. To generate the family of curve hundreds of FEA simulations are required to be carried out, which is time consuming and also requires lot of computing resource. Hence a mathematical model is more viable but to validate its predictions, FEA simulations were used as a secondary method to compare them both since FEA simulations gives fairly accurate results.

4.1 Model setup

Die was modeled as rigid body and metal and polymer were modeled as elastic-plastic materials. Material properties for metal and polymer used in simulations are listed in Table 1 below. Since ABAQUS uses values of all material and geometric properties independent of units hence all the properties listed are in SI units and consistency of

units is maintained throughout. Polymer was modeled as perfectly plastic material as can be seen for varying plastic strain the yield stress remains same. Some other parameters used for simulations are stated below -

Coefficient of friction between polymer and die – 0.1

Mass scaling factor – 1e5

Velocity – 0.01 m/s

Table 1 Material properties used for FEA simulations

Property	Plastic Strain	Metal	Polymer
Density (kg/m^3)		2700	1400
Young's Modulus (Pa)		6.90E+10	8.90E+09
Poisson's Ratio		0.33	0.33
Yield strength (Pa)	0	6.00E+07	8.00E+07
Yield strength (Pa)	0.125	9.00E+07	8.00E+07
Yield strength (Pa)	0.25	1.13E+08	8.00E+07
Yield strength (Pa)	0.375	1.24E+08	8.00E+07
Yield strength (Pa)	0.5	1.33E+08	8.00E+07
Yield strength (Pa)	1	1.65E+08	8.00E+07
Yield strength (Pa)	2	1.66E+08	8.00E+07

4.1.1 Meshing

As the nature of problem was axisymmetric hence only two dimensional model demonstrating cross section was created. Mesh used was also two dimensional with quadrilateral elements covering radial and longitudinal directions. The quadrilateral elements were varying widely in sizes, with small elements used where large strains

were anticipated and vice versa. In axisymmetric extrusion through conical die the farther the material is away from central axis the larger the strain would be; hence elements closer to die were much smaller as compared to ones closer to central axis. This was achieved by using biased meshing. The polymer material was meshed with quadrilateral elements of fine size. The details of meshing are shown below in Figure 11.

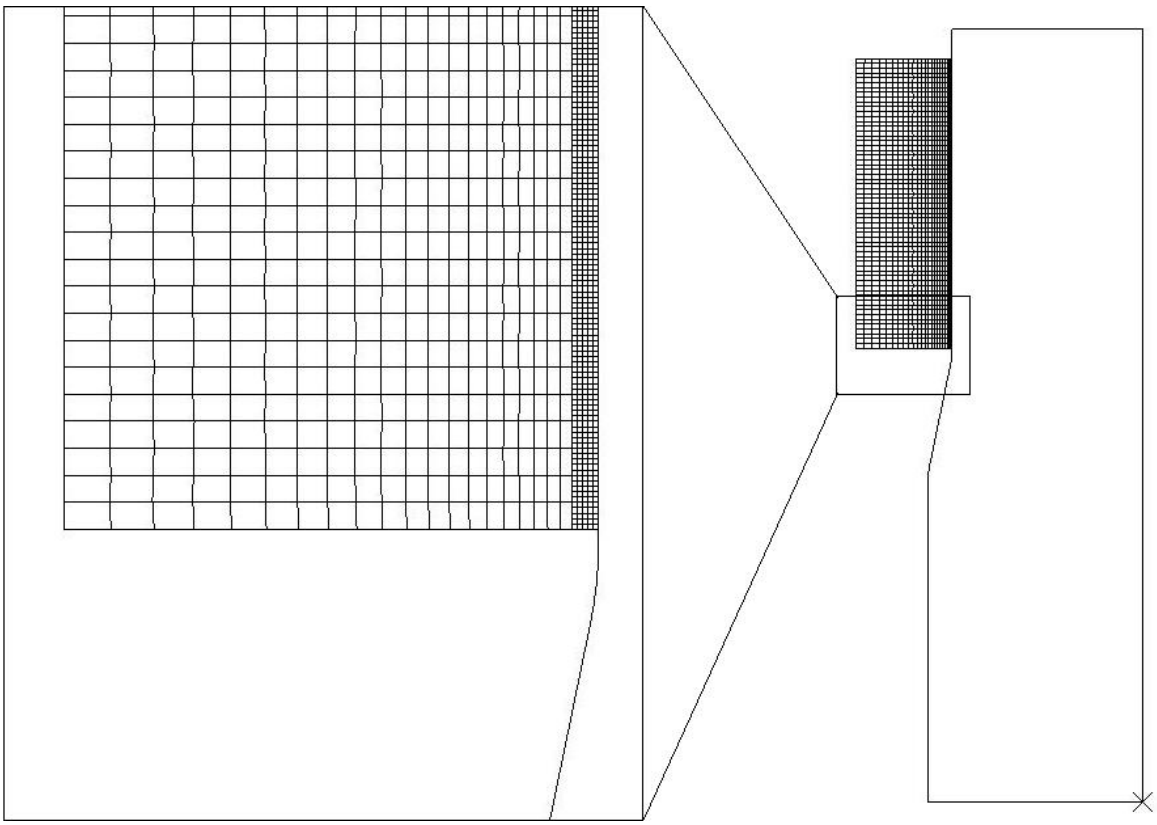

Fig. 11 Biased mesh details

4.1.2 Adaptive meshing

ABAQUS uses updated Lagrangian finite element formulation, where mesh deforms as the material deforms, after each iteration. This poses problems when there are large material deformations because mesh gets heavily distorted and job aborts. Even applying distortion control doesn't help to contain the large distortion of mesh and preventing the job from aborting. Hence to solve this problem adaptive meshing was used. For large deformations of material adaptive meshing maintains high quality mesh throughout an analysis by allowing the mesh to move independently of the material. Hence adaptive meshing only moves the nodes while mesh topology (i.e. elements and connectivity) remains the same [32]. But adaptive mesh domain is supported in the step module only for ABAQUS/Explicit analyses. Hence even though the problem of polymer coated metal rod extrusion is of quasi-static nature ABAQUS/Explicit solver was used during the simulations. Also ABAQUS/Explicit has the ability to handle the nonlinear effects of complex contact problem well [32].

4.1.3 Mass scaling

Another problem that was faced during simulations was it was taking long time of over one hour to complete the FEA simulation. Since the computing resources available at the research facility in Texas A&M University allowed only 20 min of interactive session hence it necessitated to submit the simulation in batch jobs, which takes quite a few

hours waiting in the queue before its processing starts. Mass scaling is often used in ABAQUS/Explicit for improved computational efficiency and hence it was used to achieve less time consuming and economical solution. Because element stiffness matrix in the equilibrium equation plays an important role determining efficiency and accuracy, hence mass scaling factor must be chosen so that it does not alter the solution significantly. Too low a mass scaling factor results in long run times and too high distorts the results completely. Fixed mass scaling factor applied to whole model should be chosen such that kinetic energy in the model should be small as compared to total energy. To verify this test a mass scaling factor of 1e5 was used and the kinetic energy was found to be less than 1% of total energy. Also density was increased 10 times from 2700 kg/m^3 to 27000 kg/m^3 and simulation was run again to check if the mass kinetic energy is having significant impact on the total work done, which was not the case. Results of the two simulations are given below in Figure 12.

To carry out same simulations for different die angles a parametric study was performed. Parametric study was implemented using a script that had python Lutz [33] instructions to generate and execute parametrized input file for different parameter value. Python script and the corresponding parametrized ABAQUS input file are given in Appendix III along with the major control cards in the ABAQUS input file; neglecting the geometry details and node and element definition in the input file.

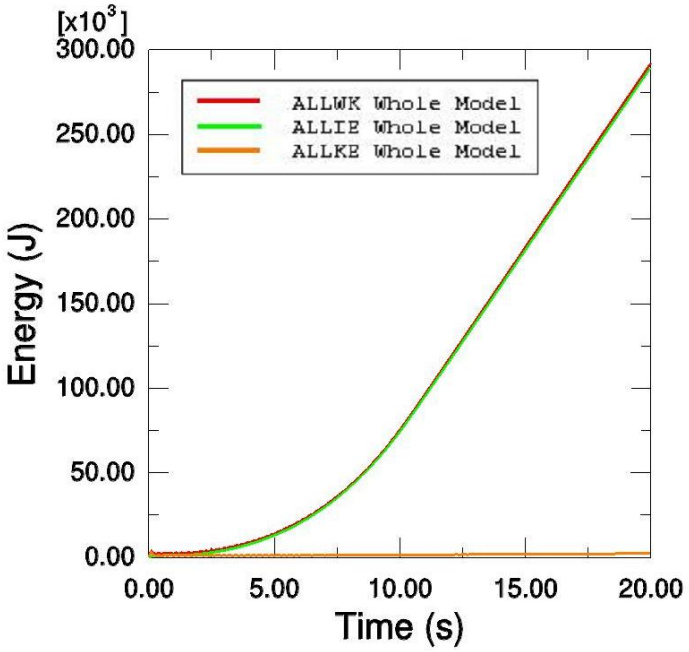

(a)

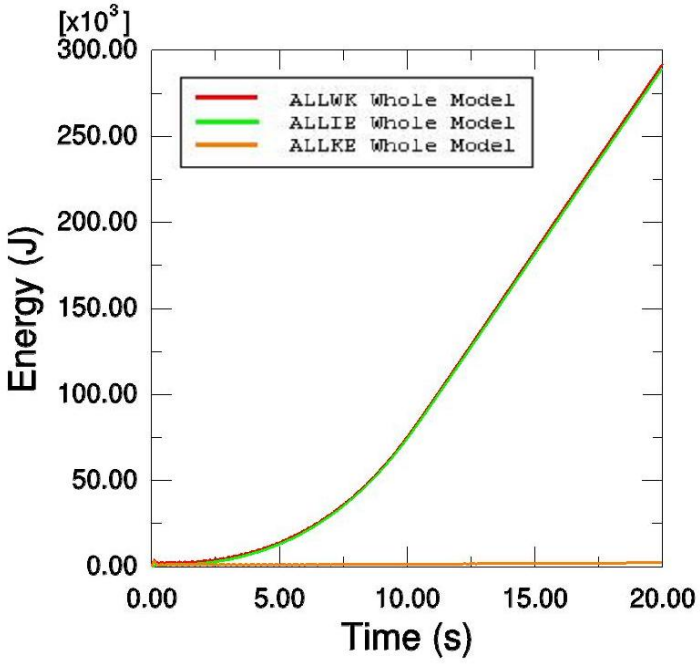

(b)

Fig. 12 Change in kinetic energy as compared to internal energy and total work for (a) mass scaling 1e5 (b) density increased 10 times along with mass scaling 1e5

4.2 Preliminary simulation

Due to dynamic nature of the problem it is important to conduct some preliminary FEA simulation of simple metal rod extrusion through conical die and verify with already published results. This is important to demonstrate simulation capability and accuracy of the setup of problem. Also it helps to solve the problems encountered with relatively simple model and in general builds confidence in using ABAQUS for our composite rod extrusion.

Two simulations were carried out for validation purpose. First was successful extrusion of bare metal rod without any coating present and second was to demonstrate center bursting failure in the simple metal rod extrusion. In simple extrusion reduction ratio was 2.0, die angle was 26°57', flow stress of metal was taken as 166 MPa and friction factor was assumed as 0.1. Results using FEA simulations and Avitzur's [5] mathematical model are compared below in Table 2. As can be seen from Table 2 the two results were comparable. Avitzur [5] developed criteria for center bursting and developed plots showing the criteria for various reduction ratio and various friction factor as the die angle changes as shown in Figure 13. In Figure 13 for a particular friction factor, area above the respective solid line is the region for successful extrusion and area below it is the region where center bursting failure occurs. When the successful extrusion simulation carried in this study was plotted on the chart it was well in the safe range as shown by the point marked in green on Figure 13.

Table 2 Comparison of extrusion pressure predicted by FEA simulations and Avitzur's [5] mathematical model

	FEA Simulations	Avitzur's mathematical model [5]
Extrusion Pressure (MPa)	320.22	357.46

Second simulation was carried out to show central bursting as predicted by the criterion developed by Avitzur [5], which is shown in Figure 13 below. In this case a metal rod of initial diameter 100 mm was reduced to 70 mm giving the reduction ratio as 1.42. Die angle used was 24° and friction factor used was 0.1 and it is marked in red on Figure 14 below. Hence as per the criteria, extrusion carried out with these process parameters should have center bursting failure and FEA simulations predicted the same result. Figure 14 (a) and (b) shows the velocity and shear stress profile respectively for the extrusion carried out with given process parameters. It is noticed that velocity and shear stress of the work material at the central axis is varying widely at regular intervals which would cause to produce voids in material at regular intervals along the axis and this phenomenon is known as center bursting.

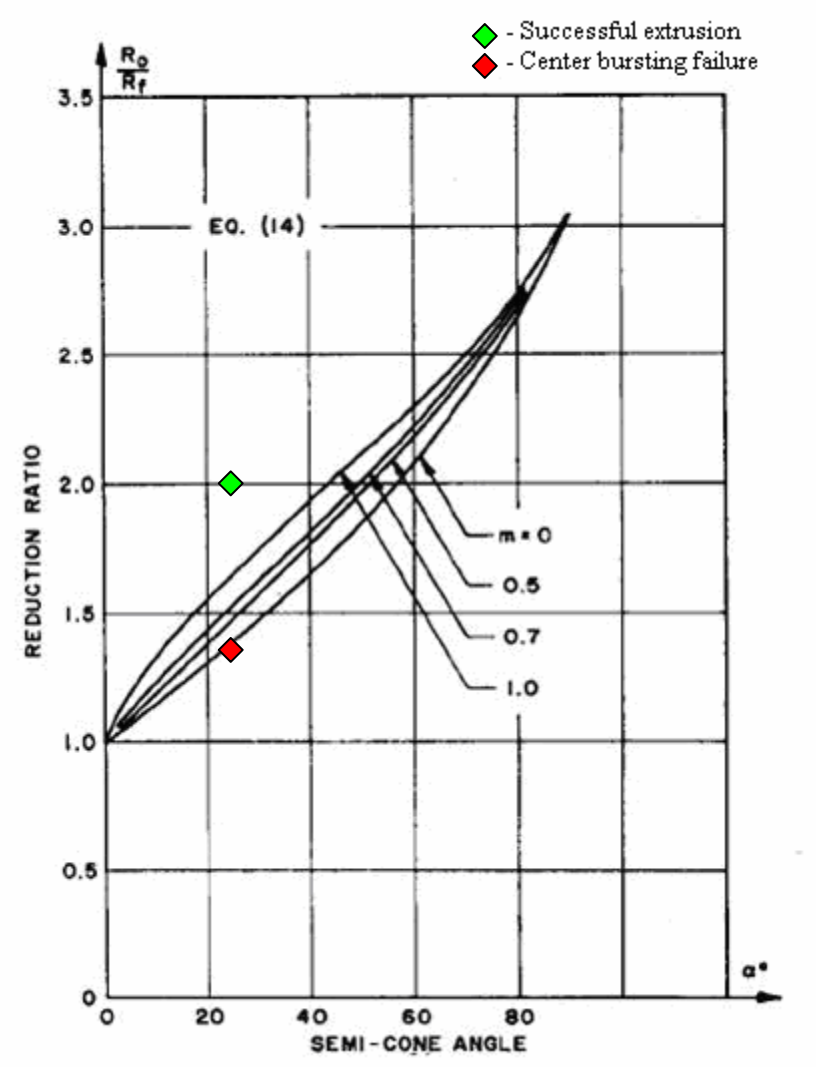

Fig. 13 Center bursting criteria developed by Avitzur [5]

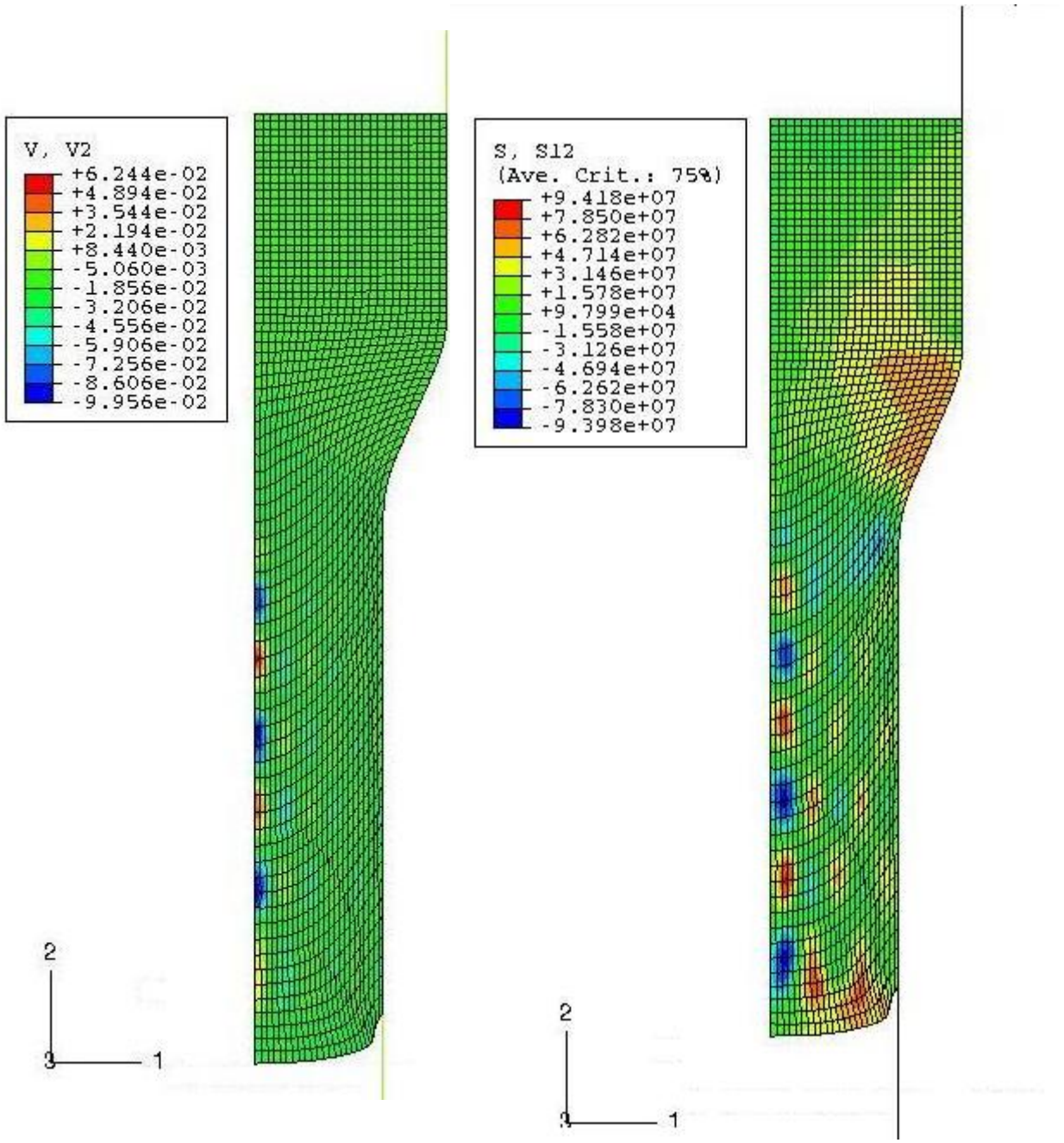

(a) **(b)**

Fig. 14 Center bursting phenomenon (a) velocity plot (b) shear stress plot

4.3 Velocity field

While carrying out polymer coated metal rod extrusion one more interesting thing found was the velocity profile of successful extrusion as shown in Figure 15 below. Velocity is constant before entering the conical die and after exiting it also. And the velocity gradient can clearly be seen as curved inwards instead of straight line or spherical in nature which is similar to the mathematical model developed in this study.

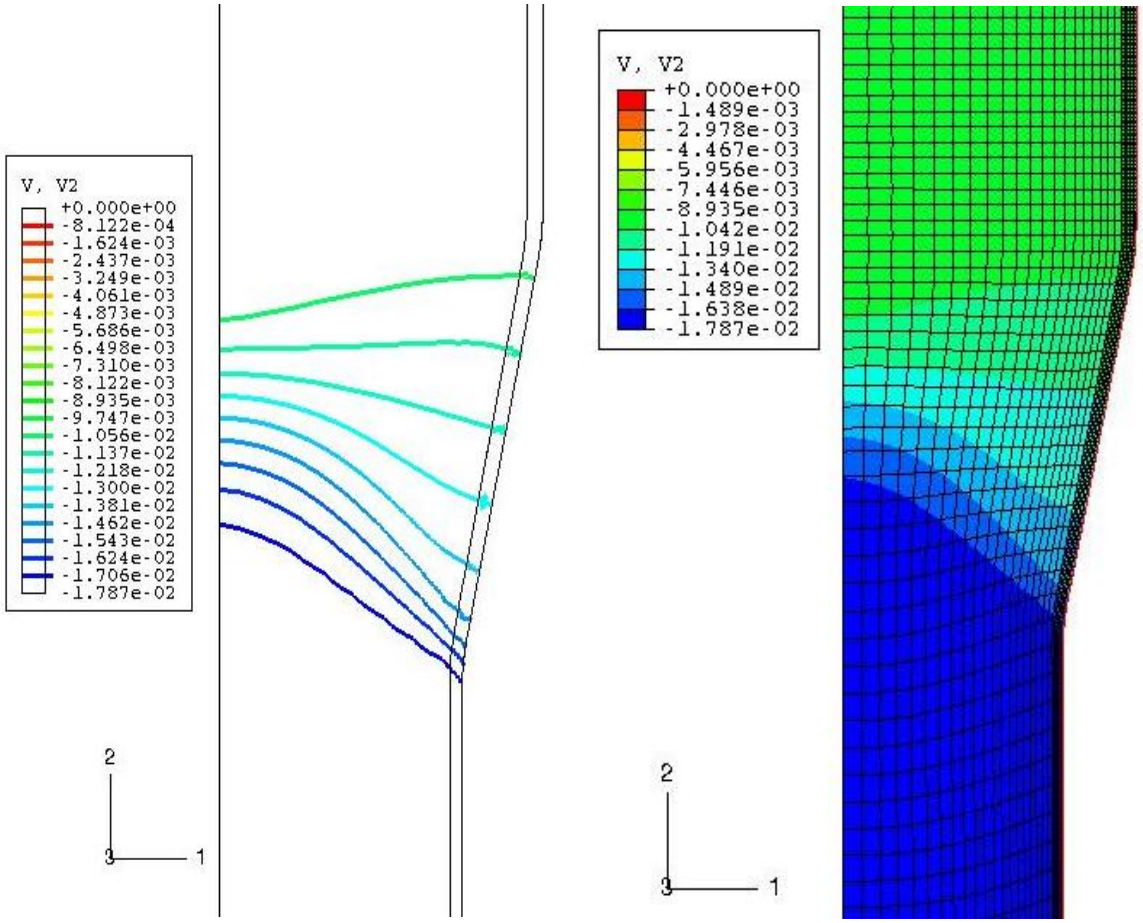

Fig. 15 Velocity gradient during polymer coated metal rod extrusion

CHAPTER V

DISCUSSION OF RESULTS

The extrusion force predicted by mathematical model for various die angles is compared with FEA simulation results in Figure 16. The mathematical model is in good agreement with FEA simulations results.

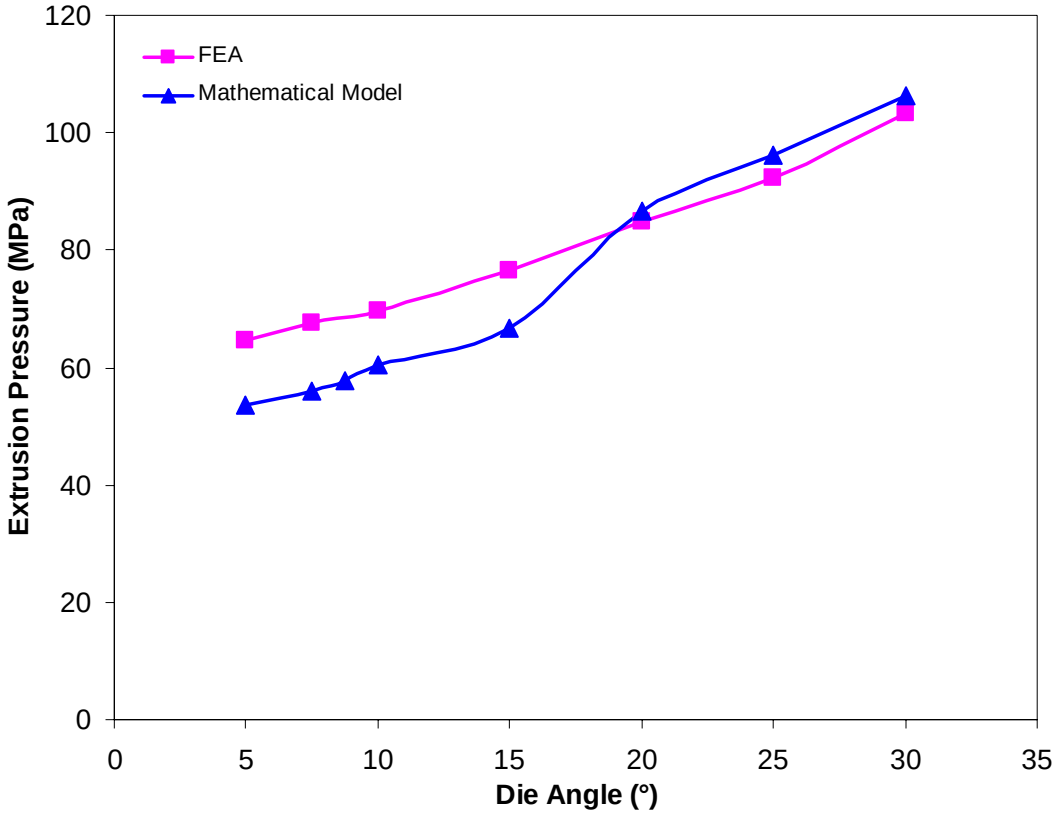

Fig. 16 Comparison of extrusion force predicted by mathematical model and FEA simulations for various die angles. Other parameters: Velocity = 10 mm/s, Friction factor = 0.1, Initial coating thickness = 5%, Reduction Ratio = 1.33

Using 100 mm as initial radius might be of concern since extrusion of such a large radii rod is not very frequent in real world. Hence a study was performed to verify if the extrusion pressure predicted by the mathematical model developed in this study was the constant if a smaller initial radius was to be used. Hence a polymer coated metal rod of Initial radius 10 mm was extruded to final radius of 7.5 mm keeping the reduction ratio same as 1.33. Keeping the other parameters same, extrusion pressure was determined and compared with the extrusion pressure predicted by taking 100 mm initial radius. The two results are given in Table 3 below and are in good agreement. Hence we can be confident in using the extrusion pressure given in Figure 16.

Table 3 Comparison of extrusion pressure predicted by mathematical model for Initial Radius 100 mm and 10 mm. Other parameters are: α = 15°, Reduction ratio = 1.33, Initial coating thickness = 5%, m = 0.1

	Initial Radius = 100 mm	Initial Radius = 10 mm
Extrusion Pressure (MPa)	66.59	60.76

The process of optimization to obtain minimum power also determines the value of the lengths defining the nature of rigid plastic deformation boundaries and also establishes the final polymer coating thickness. The variation in the four normalized lengths with respect to the die length for various die angles is shown in Figure 17 below. Significance of this chart lies in the fact that as the value of four lengths L_{oi}, L_{of}, L_{mi} and L_{mf} varies the nature of rigid plastic deformation boundaries changes substantially.

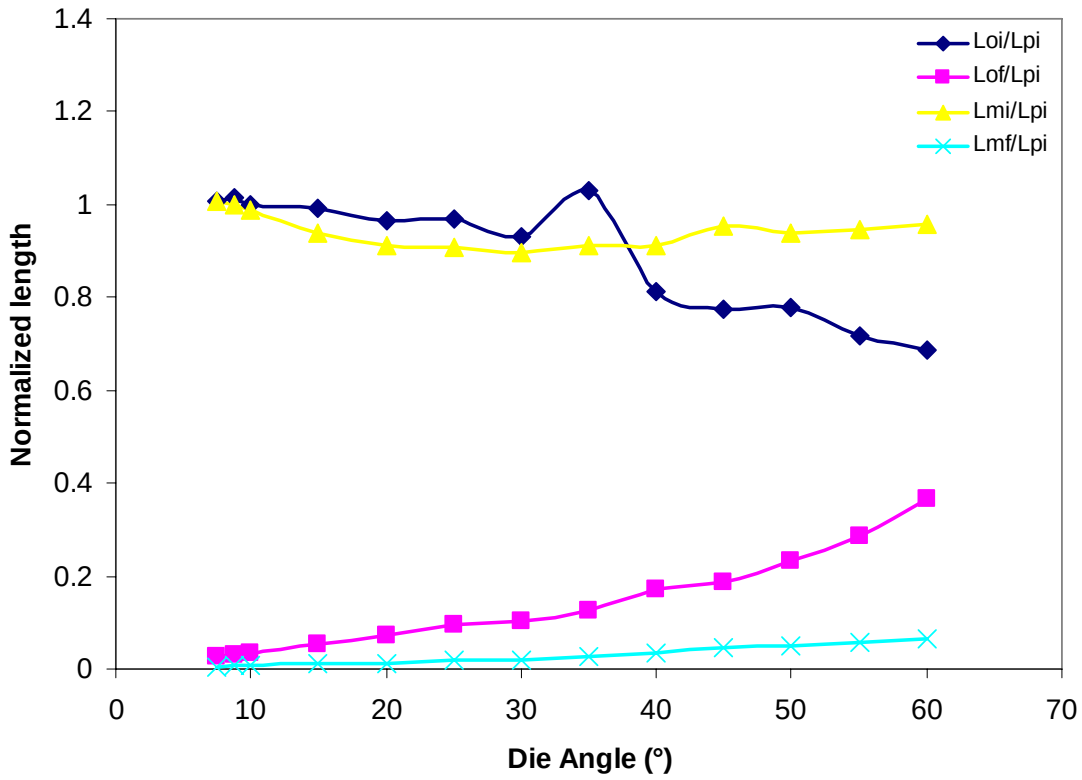

Fig. 17 Comparison of all the normalized length for various die angles

To demonstrate a case in point, consider the values of normalized lengths for die angle 20°. The nature of rigid plastic deformation boundary for the stated case is shown in Figure 18. On the other hand consider the values of normalized lengths for die angle 45° and the nature of rigid plastic deformation boundary for it is shown in Figure 19. It can be seen that the two deformation boundaries are substantially different from each other. In Figure 18 the deformation boundary at entry of die is curved outwards, whereas in Figure 19 the deformation boundary at entry of die is seen to be curved inwards.

This change in deformation boundary is emphasized in Figure 17 by the intersection point of normalized length L_{oi} and L_{mi} which occurs approximately at die angle of 38°. For all the die angles lower than die angle of 38° the rigid plastic deformation boundary at entry of die is curved outwards similar to one shown in Figure 17. And for all the die angles greater than die angle of 38° the rigid plastic deformation boundary at entry of die is curved inwards similar to one shown in Figure 18. For the die angle where L_{oi} intersects L_{mi} (i.e. approximately 38° in this case) the deformation boundary would be exactly a straight line. This shows that mathematical model developed in this study is flexible to determine the shape of velocity field on its own while minimizing the upper bound power functional. This is very important as upper bound method results are only as good as the velocity field assumed and this method has the capability to find the boundaries.

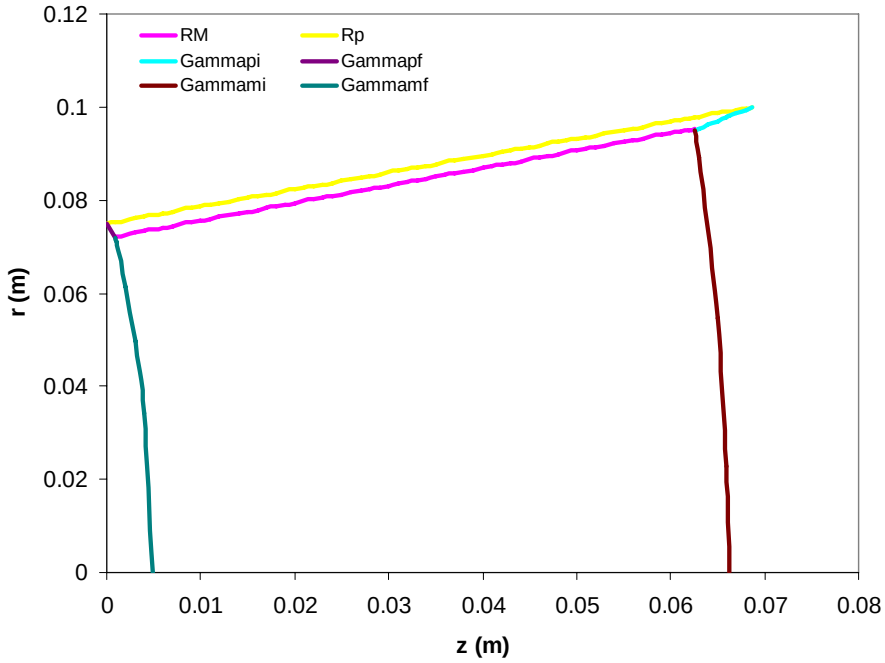

Fig. 18 Rigid plastic deformation boundaries for die angle 20°

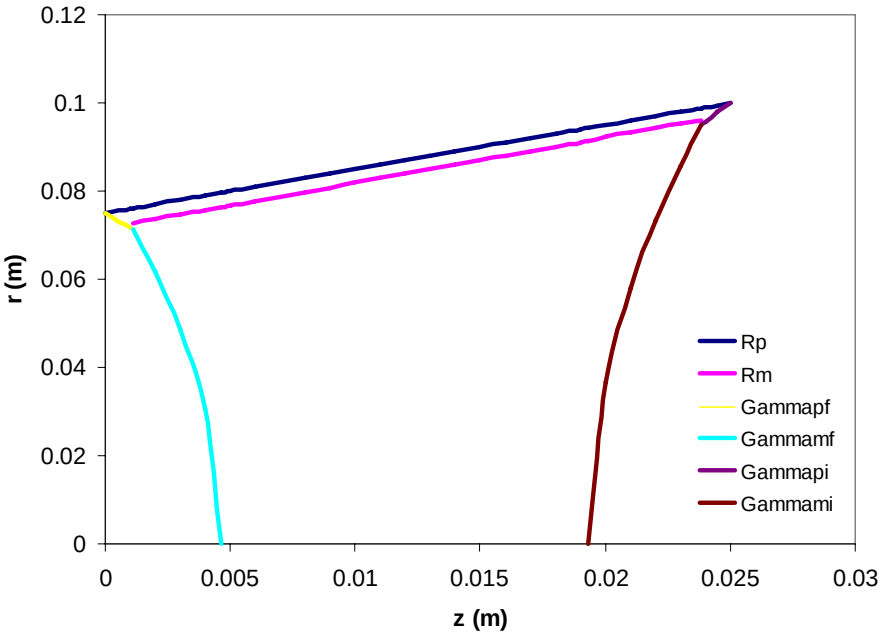

Fig. 19 Rigid plastic deformation boundaries for die angle 45°

While minimizing the upper bound power functional another parameter that is optimized along with the four lengths discussed above is the final coating thickness. Variation in final coating thickness for various die angles is shown in Figure 20. It is clearly seen that the final coating thickness is not in the same proportion as that of initial coating thickness to initial rod diameter, which seems logical too as it is being squeezed on both sides by work material and die material i.e. two metals. For die angle below 11.5° tendency of the polymer coating is to thicken which as practically is not possible. Hence below 11.5° the final coating thickness would be close to the initial coating thickness i.e. 5 mm in this case. For die angle above 16° the final coating thickness is much less than given by the fixed ratio of initial thickness to initial rod diameter. The effect of this can be detrimental as the exit velocity of polymer is greater than that of metal because from principle of mass flow rate we have

$$V_{pf} = \frac{V_{pi} t_i^2}{t_o^2} \tag{94}$$

$$V_{mf} = \frac{V_{mi} R_{mi}^2}{R_{mf}^2} \tag{95}$$

Hence there is a tendency of the polymer to rush ahead of the metal at the exit of die. If the difference between two velocities is too high, it might result in cohesive or adhesive failure of polymer coating as shown in Figure 4 and Figure 5 respectively. If the energy imparted to polymer due to added velocity is greater than the shear stress of polymer then polymer would have a cohesive failure. But if adhesive force between polymer and metal is less than the shear stress than adhesive failure would be predominant mode.

Based on this fact a failure criterion can be developed and the capability of this mathematical model can be demonstrated.

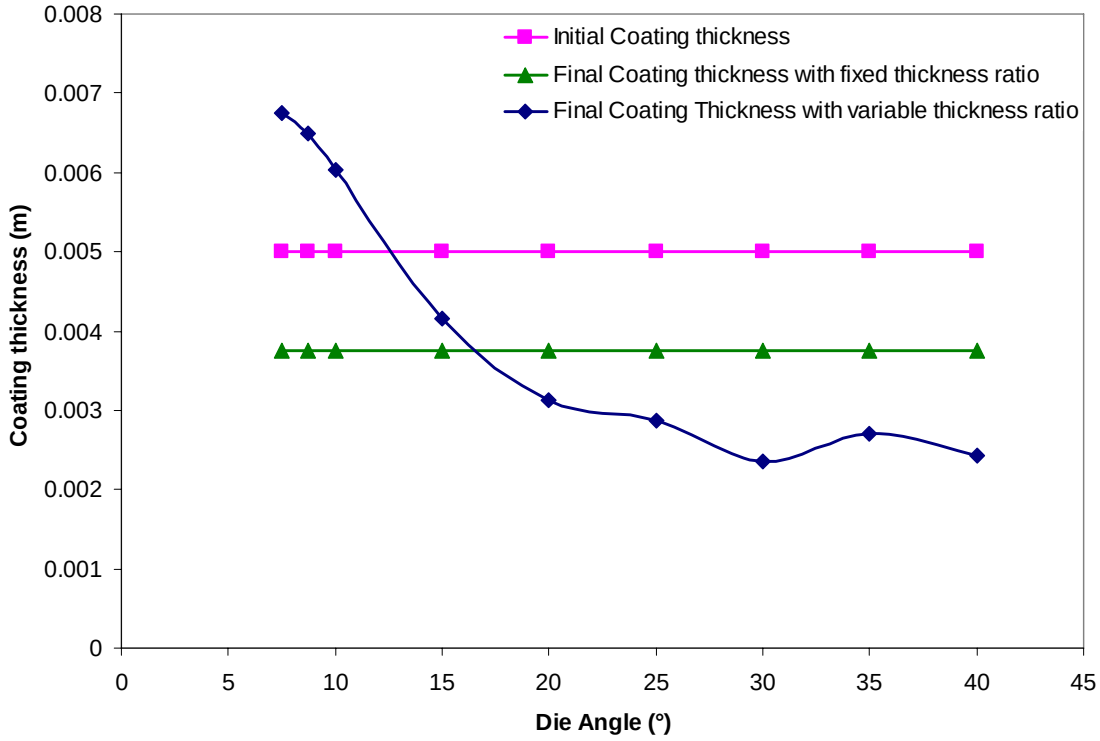

Fig. 20 Variation in final coating thickness for various die angles

The mathematical model for successful extrusion and adhesive failure of extrusion developed can be utilized to determine some important results such as critical die angle for polymer coated metal rod extrusion to be successful. A comparison between the extrusion pressure required for successful extrusion and for adhesive failure of polymer coating during extrusion is shown in Figure 21. It is clearly shown that below a certain die angle called critical die angle power required for successful extrusion is less than

power required for adhesive failure of extrusion and hence is the preferred mode according to the limit theorem of Drucker et. al. [34]. The critical angle in this case is 12° and above this die angle the adhesive failure would require less power as compared to successful extrusion and hence will be the dominant mode. With knowledge of various process parameters like reduction ratio, initial coating thickness, velocity and material properties critical die angle can be determined mathematically. Family of such curves could be generated to give critical die angle for various set of process parameters, which could be proved to be very useful for designing the polymer coated metal rod extrusion.

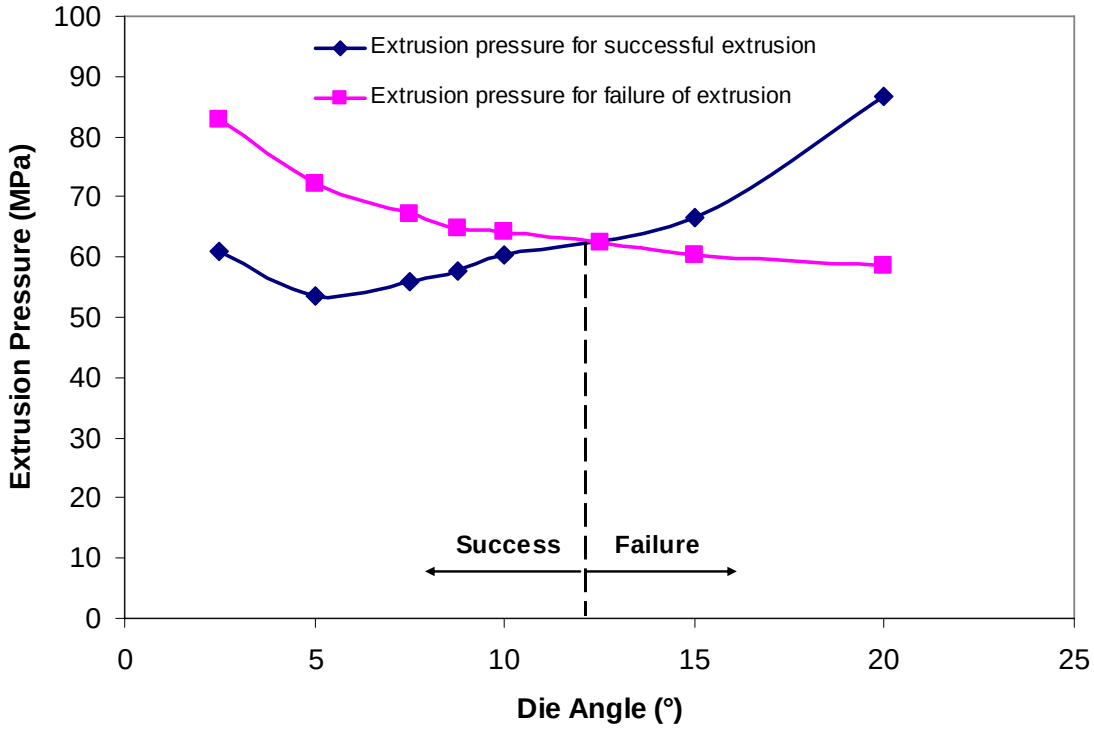

Fig. 21 Comparison of extrusion pressure required for extrusion for failure and successful extrusion of polymer coated metal rod. Parameters are: Reduction Ratio = 1.33, V_i = 10 mm/s, initial thickness = 5%

To verify the theoretical results FEA simulations were carried out at various die angles for same process parameters and indication of failure were found for die angle in the range of 11.77° - 15°. Figure 22 shows result of FEA simulation for die angle 11.77° and it can be clearly seen that there is uniform von-Mises stress in polymer coating and hence no indication of failure. Whereas Figure 23 shows result of FEA simulation for die angle 15° and it is seen that von-misses stress in polymer coating is not uniform and has repetitive high and low stress which will indicates the polymer will fail.

One important observation that is noted here is due to polymer coating the range of process parameters for successful extrusion is reduced. If we see the center bursting chart developed by Avitzur [5] as shown in Figure 5 for reduction ratio of 1.33 the maximum die angle for which extrusion is successful is around 20°. Whereas for polymer coated metal rod extrusion the critical angle reduces to around 12°. Hence it can be deduced that polymer coating reduces the range of die angle for the polymer coated metal rod extrusion to be successful as compared to bare metal rod extrusion.

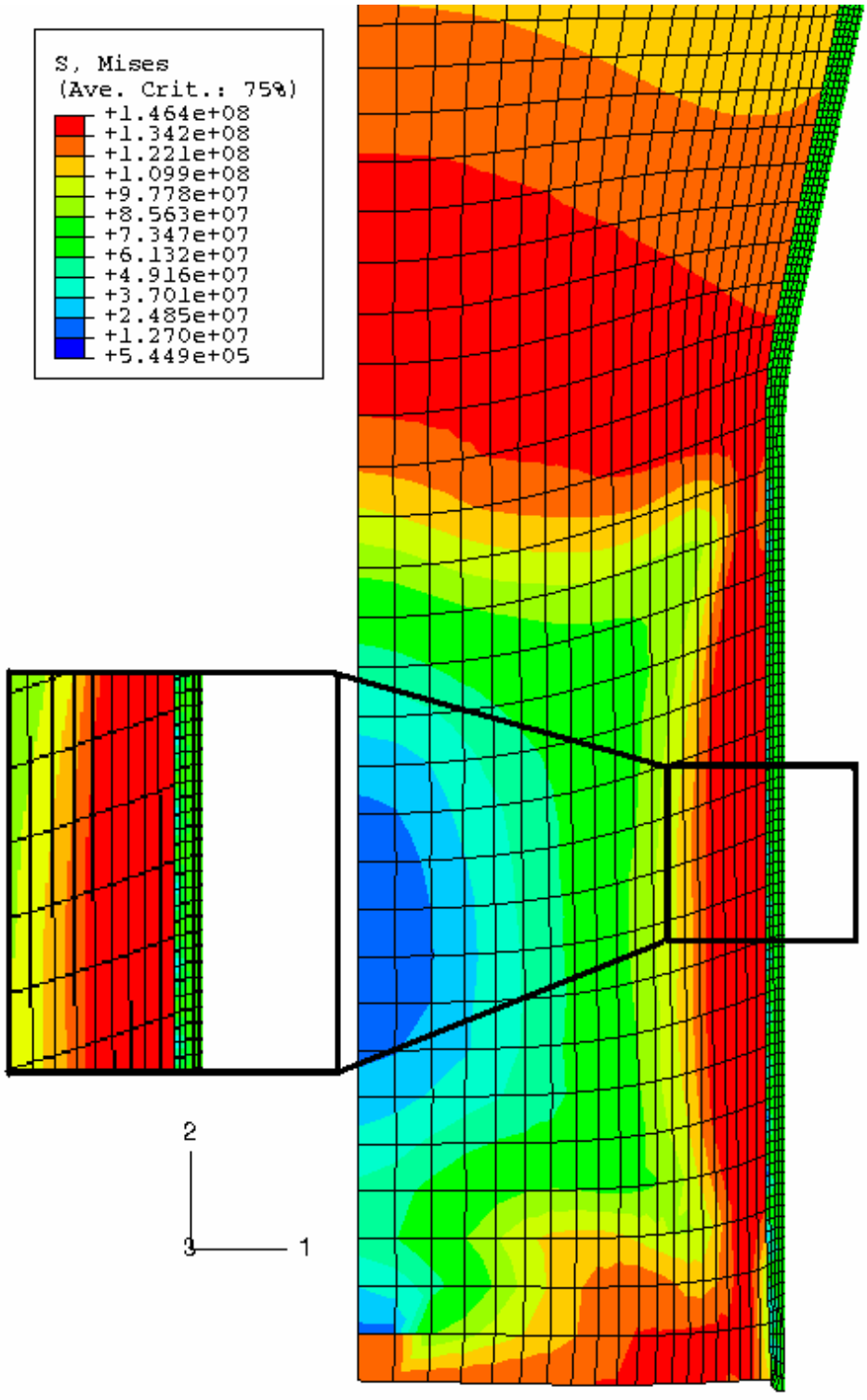

Fig. 22 Results of FEA simulation at die angle 11.77° with zoomed section. Other parameters are: Reduction ratio = 1.33, V_i = 10 mm/s, t_i = 5 mm, m_p = 0.1

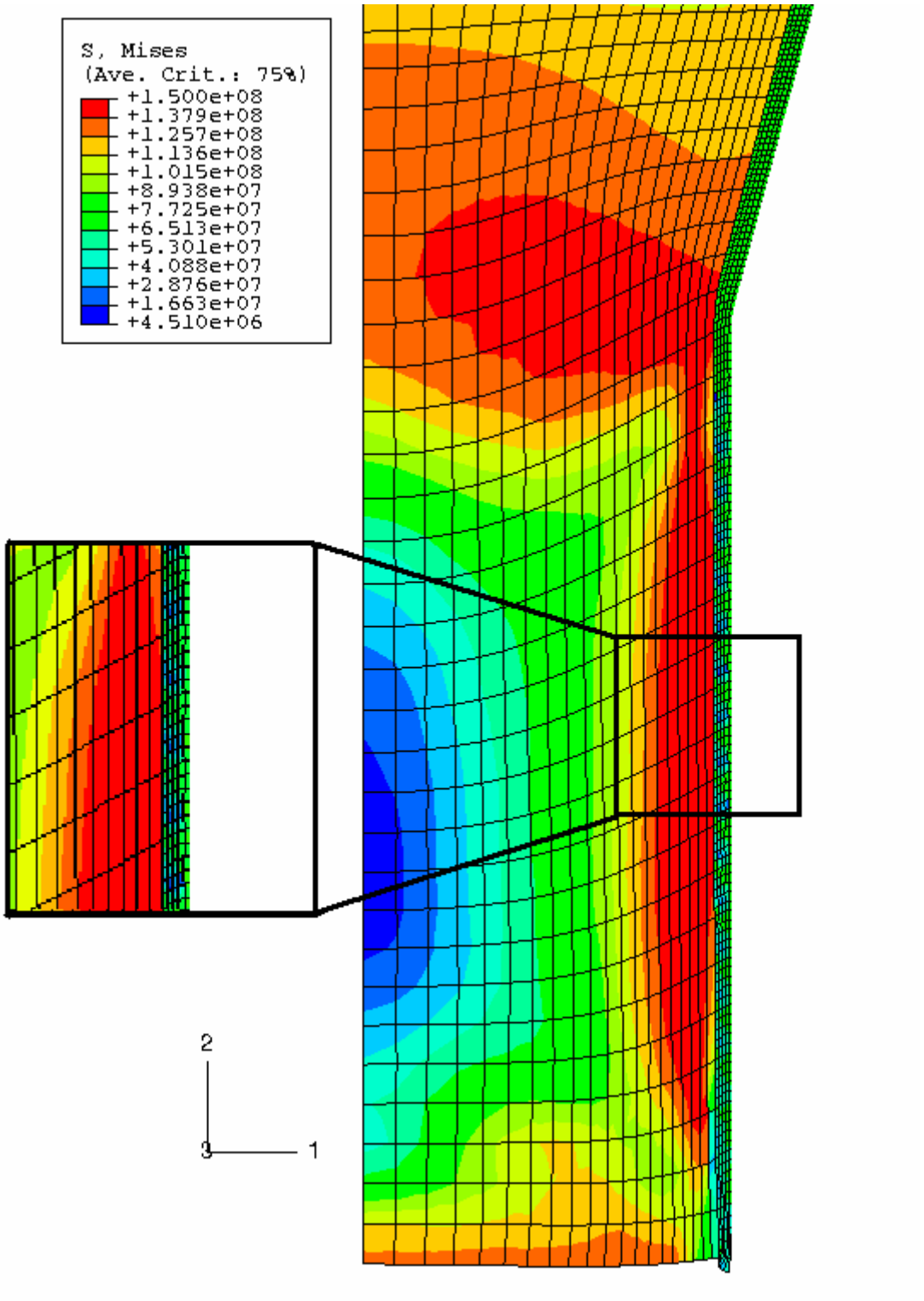

Fig. 23 Results of FEA simulation at die angle 15° with zoomed section. Other parameters are: Reduction ratio = 1.33, V_i = 10 mm/s, t_i = 5 mm, m_p = 0.1

Variation in power required for extrusion for various initial coating thickness is shown in Figure 24 below. Power remains fairly constant for initial polymer coating thickness upto 10% of total incoming diameter but falls rapidly thereafter. This seems logical as polymer has lower flow stress as compared to that of metal and hence power required to plastically deform polymer would be less than metal. Variation in final coating thickness for various initial coating thicknesses is shown in Figure 25 below.

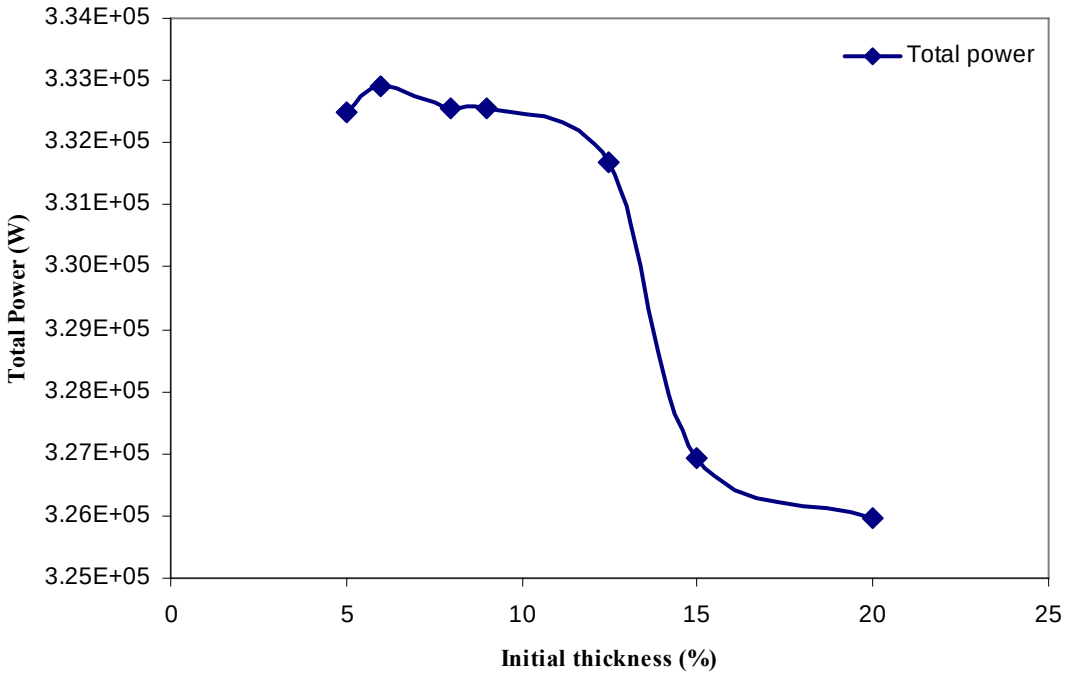

Fig. 24 Total extrusion power for various initial thickness. Other parameters are: Reduction ratio = 1.33, V_i = 10 mm/s, α = 15°, m_p = 0.1

As can be seen in Figure 25 the final coating thickness predicted by the analytical model is much less than the ratio of initial coating thickness to initial rod radius. This would impart the polymer greater velocity as compared to metal at the exit of die. This phenomenon can be seen in FEA simulations also when observed carefully. As shown in Figure 22 the polymer is trying to rush away quicker than metal coming out of exit of die and hence a small overhang can be seen. As mentioned earlier this disproportionate velocity may cause cohesive or adhesive failure of polymer at the die exit depending on the adhesive bond between polymer and metal being greater or less than the shear stress of polymer.

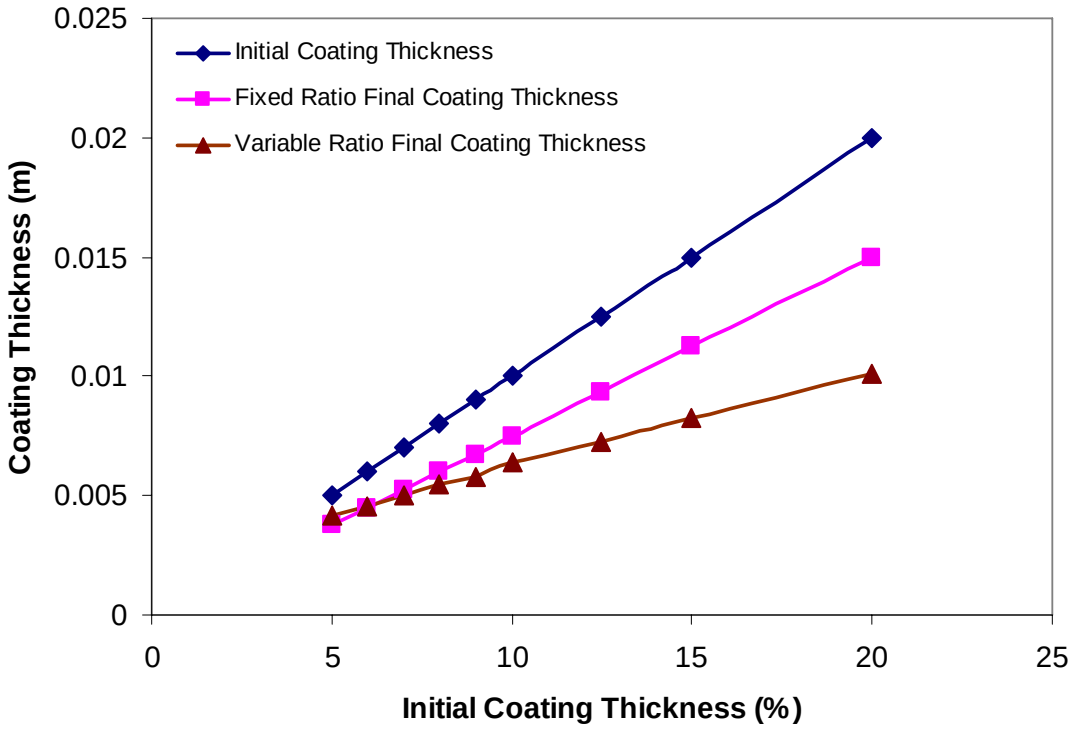

Fig. 25 Final coating thickness for varying percentage of initial coating thickness. Other parameters R_{pi} = 100 mm, R_{pf} = 75 mm, V_i = 10 mm/s, α = 15°

CHAPTER VI

CONCLUSIONS

A new mathematical model implementing upper bound method has been developed to predict extrusion pressure required to successfully carry out polymer coated metal rod extrusion. Also mathematical model was extended to incorporate adhesive failure case and it was capable to predict the extrusion pressure for adhesive failure. FEA results were in good agreement with the results predicted by mathematical model. The new mathematical model developed has following advantages –

- Simple flow functions of first order were used to develop the mathematical model to reduce the mathematical complexity but still give acceptable results. Optimization was used to minimize the upper bound power functional to determine extrusion pressure.
- Mathematical model for adhesive failure of the coating was also developed and integrated with the mathematical model for successful axisymmetric extrusion to determine the failure at certain die angle. Hence a critical angle was established for the polymer coated metal rod extrusion process. If the die angle is above the critical angle it will result in adhesive failure and if the die angle is less than critical angle the extrusion will be successful and the final product would have intact polymer coating on it.
- The upper bound power functional is modeled as unconstrained non linear optimization problem and the optimization process searches for the five

parameters to determine the nature of boundary of velocity field. The rigid plastic deformation boundaries do not have a fixed geometry and it can have widely varying profile as determined by the optimization process. Hence depending on the die angle it can be curved outside at the die entry end making it similar to Avitzur's [5] spherical velocity field or it can be curved inside at the die entry end making it similar to the velocity field developed by Hwang et. al. [26]

- By modeling the final coating thickness as one of the search parameters in optimization it was also shown that final thickness of polymer coating is not in proportion with the ratio of initial thickness to the initial radius of work piece.
- Range of die angle for the polymer coated metal rod axisymmetric extrusion to be successful reduces due to polymer coating as compared the extrusion of bare metal rod.

The results of this study are summarized below –

- Extrusion pressure predicted by the mathematical model for successful extrusion developed in this study is in good agreement with the extrusion pressure predicted by FEA simulations.
- Effect of initial radius of polymer coated metal rod used in the mathematical model to determine the extrusion pressure for a particular reduction ratio is insignificant and hence the predictions by the mathematical model are effective.

- The nature of rigid plastic deformation boundary changes at approximately 38° of die angle. For die angle below 38° the deformation boundary at the entry end is curved outside and vice versa.
- The final coating thickness is not in proportion of the initial coating thickness to initial work piece radii. Above die angle of approximately 16° the final coating thickness is much less than the original proportion and below approximately 11.5° it is almost equal to the initial coating thickness.
- Critical die angle for the study conducted was found to be 12°. As predicted by the mathematical model and FEA simulations above die angle of 12° the extrusion of polymer coated metal rod through conical die would not be successful and vice versa.
- As the initial coating thickness is increased from 5% to 20% the power required to successfully extrude the work material reduces considerably.

The future work can include conducting the experimentations to verify the extrusion pressure predicted by the mathematical model developed in this study. Parametric study can be done using the mathematical model developed to find critical angle for a range of reduction ratio. Also the mathematical model can be improved by incorporating more complex polymer behavior and the thermal effects as a result of the heat generated due to the polymer coated metal rod extrusion process.

REFERENCES

[1] Schey, J. A., 1984, *Tribology in Metalworking: Friction, Lubrication and Wear*, American Society of Metals, Metals Park, OH.

[2] Rao, U. S., 1967, "Polyethylene as a Lubricant for Deep Drawing," Sheet Metal Industries, **44**, pp. 673-678.

[3] Mear, D. R., Topper, H. H., 1963, "Plastics as Lubricants for Deep Drawing and Presswork," Sheet Metal Industries, **40**, pp. 567-570.

[4] Groover M. P., 1996, *Fundamentals of Modern Manufacturing: Materials, Processes and Systems*, John Wiley & Sons Inc., New York, NY.

[5] Avitzur, B., 1968, "Analysis of Central Bursting in Extrusion and Wire Drawing," Journal of Engineering for Industry, **90**, pp. 79-91.

[6] Hosford W. F., Cadell R. M., 1983, *Metal Forming Mechanics and Metallurgy*, Prentice-Hall Inc., Englewood Cliffs, NJ, pp. 143 – 149.

[7] Clift, S.E., Hartley, P., Sturgess, C.E.N., Rowe, G.W., 1990, "Fracture Prediction in Plastic Deformation Processes," Int. J. Mech. Sci., **32**(1), pp. 1-17.

[8] Cockroft, M.G., Latham, D.J., 1968, "Ductility and the Workability of Metals," Journal of the Institute of Metals, **96**, pp. 33-43.

[9] Kudo, H., 1960, "Some Analytical and Experimental Studies of Axisymmetric Cold Forging and Extrusion," Int. J. Mech. Sci., **2**, pp. 102 – 127.

[10] Avitzur, B., 1966, "Analysis of Metal Extrusion," ASME J. of Eng. for Ind., **87**, pp. 57-70.

[11] Kobayashi, S., Thomsen E. G., 1965, "Upper- and Lower-Bound Solutions to Axisymmetric Compression and Extrusion Problems," Int. J. Mech. Sci., **7**, pp. 127-143.

[12] Bianchi, J. H., Sheppard, T., 1987, "A Comparison of a Viscoplastic Finite-Element Model with Slip-Line Field and Upper-Bound Solutions for Non-Hardening Material Subjected to Plane Strain and Axisymmetric Extrusion," Int. J. Mech. Sci., **29**, pp. 61-81.

[13] Zimmerman, Z., Avitzur, B., 1970, "Metal Flow through Conical Converging Dies - a Lower Upper Bound Approach Using Generalized Boundaries of the Plastic Zone," Journal of Engineering for Industry, **92**, pp.119-129.

[14] Chen, C. T., Ling, F. F., 1968, "Upper-Bound Solution to Axisymmetric Extrusion Problem," Int. J. Mech. Sci., **10**, pp. 863-879.

[15] Chang, K. T., Choi, J. C., 1971, "Upper-Bound Solutions to Extrusion Problems through Curved Dies," *Developments in Mechanics: Proc. 12th Midwestern Mech. Conf.*, **6**, University of Notre Dame, West Lafayette, IN, pp. 383-396.

[16] Nagpal, V., 1974, "General Kinematically Admissible Velocity Fields for Some Axisymmetric Metal Forming Problems," Journal of Engineering for Industry, **96,** pp. 1197-1201.

[17] Yang, D. Y., Han, C. H., Lee, B. C., 1985, "The Use of Generalized Deformation Boundaries for the Analysis of Axisymmetric Extrusion through Curved Dies," Int. J. Mech. Sci., **27**(10), pp. 653-663.

[18] Yang, D. Y., Han, C. H., 1987, "A New Formulation of Generalized Velocity Field for Axisymmetric Forward Extrusion through Arbitrarily Curved Dies," Journal of Engineering for Industry, **109,** pp. 161-168.

[19] Altan, S. B., Antar, N., Gultekin, E., 1992, "A Comparison of Some Deformation Models in Axisymmetric Extrusion," Journal of Materials Processing Technology, **33**, pp. 263-272.

[20] Alexandrov, S., Mishuris, G., Miszuris, B., Sliwa, R. E., 2001, "On the Dead-Zone Formation and Limit Analysis in Axially Symmetric Extrusion," Int. J. Mech. Sci., **43**, pp. 367-379.

[21] Osakada, K., Limb, M., Mellor, P.B., 1973, "Hydrostatic Extrusion of Composite Rods with Hard Cores," Int. J. Mech. Sci., **15**, pp. 291-307.

[22] Tayal, A. K., Natarajan, R., 1981, "A Finite Element Analysis of Axisymmetric Extrusion of Composite Rods," Int. J. Machine Tool Des., **21**(3/4), pp. 227-235.

[23] Avitzur, B., Wu, R., Talbert, S., Chou, Y. T., 1982, "Criterion for the Prevention of Core Fracture During Extrusion of Bimetal Rods," Journal of Engineering for Industry, **104**, pp. 293-304.

[24] Avitzur, B., Wu, R., Talbert, S., Chou, Y. T., 1986, "Analysis of Core Fracture in Drawing of Bimetal Rods and Wires," Journal of Engineering for Industry, **108**, pp. 133-140.

[25] Yang, D. Y., Kim, Y. G., Lee, C. M., 1991, "An Upper Bound Solution for Extrusion of Composite Rods through Curved Dies," Int. J. Mach. Tools Manufact., **31**(4), pp. 565-575.

[26] Hwang, Y.-M., Hwang, T.-F., 2002, "An Investigation into the Plastic Deformation Behavior within a Conical Die During Composite Rod Extrusion," Journal of Materials Processing Technology, **121**, pp. 226-233.

[27] Kang, C. -G., Kwon, H. C., 2002, "Finite Element Analysis Considering Fracture Strain of Sheath Material and Die Lubricant in Extrusion Process of Al-Cu Clad Composites and Its Experimental Investigation," Int. J. Mech. Sci., **44**, pp. 247-267.

[28] Jawroski, J. A., Schmid, S. R., 1999, "Survivability of Laminated Polymer Lubricant Films in Ironing", Tribology Transactions, **42**, pp. 32-38.

[29] Wilson, W. R. D., Halliday, K., 1977, "An Inlet Zone Analysis for the Lubrication of a Drawing Process by Rigid-Plastic Solid", Wear, **42**, pp. 135-148.

[30] Lagarias, J.C., Reeds, J. A., Wright, M. H., Wright, P. E., 1998, "Convergence Properties of the Nelder-Mead Simplex Method in Low Dimensions," SIAM Journal of Optimization, **9**(1), pp.112-147.

[31] Rao, S. S., 1996, *Engineering Optimization Theory & Practice*, Third Edition, John Wiley & Sons Inc., New York, NY, pp. 368-376.

[32] Editors of ABAQUS Manual, *ABAQUS/CAE User's Manual*, Hibbitt, Karlsson & Sorenson Inc.

[33] Lutz, M., 1996, *Programming Python,* O'Reilly & Associates, Inc., Bonn, Germany.

[34] Drucker, D.C., Prager, W., Greenberg, H.J., 1952, "Extended Limit Design Theorems for Continuous Media", Q. J. Appl. Math., **9**, pp. 381-389.

APPENDIX I

optimize.m

```
%================================================================
%   This is the Main program called from Matlab Interactive
%   Window and effectively calls all the other program to
%   get optimzed solution for successful extrusion as well
%   as failed extrusion.
%
%   Also it writes the initial values of all the parameters
%   and value of functional and process variables after each
%   iteration in a file named 'solution.xls' in the same
%   directory where this file is.
%================================================================
clear all;
clc;
Vi = 0.010;            % Note Ram Velocity is in mm/sec
Rpi = 0.100;           % Initial Radius
Rpf = 0.075;
RA = 1-(Rpf^2/Rpi^2);  % 50 Percent Area Reduction
Ratio_i = 0.05;        % Initial Radius Ratio
Rmi = (1-Ratio_i)*Rpi; %
alpha = 20;            % Die Angle in degrees
Lpf = 0;
Lpi = (Rpi-Rpf)/tan(deg2rad(alpha));
Rmf = Rpf-0.001
y = [Vi, Rpi, Rpf, Rmi, Lpf, Lpi,];

x0 = [Lpi-4,Lpf+4,Lpi-1,Lpf+1,Rmf]; % Initial guess Loi,Lof,Lmi,Lmf,Rmf

first = ['Loi' , 'Lof', 'Lmi', 'Lmf', 'Rmf', 'Vi', 'Rpi', 'RA', 'Rpf',
'Ratio', 'Rmi', 'Alpha', 'Lpf', 'Lpi'];
second = [x0(1), x0(2), x0(3), x0(4), x0(5), 0, Vi, Rpi, RA, Rpf,
Ratio_i, Rmi, alpha, Lpf, Lpi];
dlmwrite('solution.xls',first,'\t');
dlmwrite('solution.xls',second,'-append','delimiter','\t','newline',
'pc');
options = optimset('OutputFcn',
@outfun,'Largescale','off','Display','iter','MaxFunEvals',100,'MaxIter'
,50,'TolFun',1e+3,'TolX',0.001);
[x,fval,exitflag,output] = fminsearch(@(x) fun(x,y),x0,options);

sol = [x(1), x(2), x(3), x(4), x(5), fval];
dlmwrite('solution.xls',sol,'-append','delimiter','\t','newline','pc');
```

fun.m

```
function J = fun(x,y)
%=============================================================
%   This is the function called by optimize.m and calcualted
%   total upper bound power by summing all its components
%
%   It calls various other functions to obtain the value of
%   components of total power.
%=============================================================
syms r z real;

global Vi Rpi Rpf Rmi Lpf Lpi Loi Lof Lmi Lmf Rmf;

% Known values
Vi = y(1);
Rpi = y(2);
Rpf = y(3);
Rmi = y(4);
Lpf = y(5);
Lpi = y(6);

% unknown values passed as arguments
Loi = x(1);
Lof = x(2);
Lmi = x(3);
Lmf = x(4);
Rmf = x(5);

% Flow Stress values from abaqus simulation -
Sigmam = 166e6;
Sigmap = 80e6;

% coefficient of friction values
mm = 0;
mp = 0.1;

% Part I of Energy dissipated due to internal deformation in Metal
z1 = Lof;
z2 = Loi;
Rlo = 0;
Rhi = 'Rm';
fnc = 'Wim';
Wim1 = DblIntg(fnc,Rlo,Rhi,z1,z2,0.01)

% Part II of Energy dissipated due to internal deformation in Metal
z1 = Lmf;
z2 = Lof;
Rlo = 'Gammamf';
Rhi = 'Rm';
Wim2 = DblIntg(fnc,Rlo,Rhi,z1,z2,0.01)
```

```
% Part III of Energy dissipated due to internal deformation in Metal
z1 = Loi;
z2 = Lmi;
Rlo = 'Gammami';
Rhi = 'Rm';
Wim3 = DblIntg(fnc,Rlo,Rhi,z1,z2,0.01)

% Total Energy dissipated due to internal deformation in Metal
Wim = (2*pi*Sigmam/sqrt(3))*((Wim1) + (Wim2) + (Wim3))

% Part I of Energy dissipated due to internal deformation in Polymer
z1 = Lmf;
z2 = Lmi;
Rlo = 'Rm';
Rhi = 'Rp';
fnc = 'Wip';
Wip1 = DblIntg(fnc,Rlo,Rhi,z1,z2,0.01)

% Part II of Energy dissipated due to internal deformation in polymer
z1 = Lpf;
z2 = Lmf;
Rlo = 'Gammapf';
Rhi = 'Rp';
Wip2 = DblIntg(fnc,Rlo,Rhi,z1,z2,0.01)

% Part III of Energy dissipated due to internal deformation in polymer
z1 = Lmi;
z2 = Lpi;
Rlo = 'Gammapi';
Rhi = 'Rp';
Wip3 = DblIntg(fnc,Rlo,Rhi,z1,z2,0.01)

% Total Energy dissipated due to internal deformation in Polymer
Wip = (2*pi*Sigmap/sqrt(3))*((Wip2) + (Wip3) + (Wip1))

% Total energy dissipated due to internal deformation
Wi = Wim + Wip

% Energy dissipated due to frictional losses at polymer-die interface
z1 = Lpf;
z2 = Lpi;
fnc = 'DeltaVRp';
Wfp = (2*pi*mp*Sigmap/sqrt(3))*quadl(fnc,z1,z2);

% Energy dissipated due to frictional losses at polymer-metal interface
z1 = Lmf;
z2 = Lmi;
fnc = 'DeltaVRm';
Wfm = (2*pi*mm*Sigmam/sqrt(3))*quadl(fnc,z1,z2);

% Total energy dissipated due to frictional losses
Wf = (Wfp) + (Wfm)
```

```
% Energy dissipated due to shear losses at boundary Gammami
z1 = Loi;
z2 = Lmi;
fnc = 'DeltaVmi';
Wsmi = 2*pi*Sigmam/sqrt(3)*quadl(fnc,z1,z2)

% Energy dissipated due to shear losses at boundary Gammamf
z1 = Lmf;
z2 = Lof;
fnc = 'DeltaVmf';
Wsmf = 2*pi*Sigmam/sqrt(3)*quadl(fnc,z1,z2)

% Energy dissipated due to shear losses at boundary Gammapi
z1 = Lmi;
z2 = Lpi;
fnc = 'DeltaVpi';
Wspi = 2*pi*Sigmap/sqrt(3)*quadl(fnc,z1,z2)

% Energy dissipated due to shear losses at boundary Gammapf
z1 = 0;
z2 = Lmf;
fnc = 'DeltaVpf';
Wspf = 2*pi*Sigmap/sqrt(3)*quadl(fnc,z1,z2)

% Total energy dissipated due to shear losses
Ws = (Wsmi) + (Wsmf) + (Wspf) + (Wspi);

% Total Power using upper bound method
J = Wi + Wf + Ws
```

DblIntg.m

```
function a = DblIntg(fnc,Rlo,Rhi,z1,z2,tol)
%============================================================
%   function DblIntg executes a double integral of the function
%   'fnc' over the limits z1<z<z2, Rlo(z)<r<Rhi(z).  The limits
%   on the r integration can be either scalars or functions of
%   z.  The function calls function 'G2d', which executes a 1-d
%   integration over r for each value of z.
%
%   If the integration limits of the inner integral (over r) are
%   functions of z, the user must supply functions called 'Rhi'
%   and 'Rlo'.  Otherwise, simple numerical values can be used.
%
%   The limits of the outer integral (over z) must be scalars.
%
%   The integrand function, fnc(r,z), is a user-supplied function
%   of two variables.  The name of this function, enclosed in
%   single quotes, is the first element of the argument list.
%
%   The accuracy is determined by the tolerance, tol.  If
```

```
%   omitted, a value of tol = 1.e-3 is used.
%
%   The use is
%
%        a = DblIntg(fnc,'Rlo','Rhi',z1,z2,tol)
%============================================================
  if nargin < 6;
      tol=1.e-3;
  end;
  tl=tol;
  a = quadl('G2d',z1,z2,tol,0,Rlo,Rhi,fnc,tl);
```

G2d.m

```
function f = G2d(z,R1,R2,fnc,tl)
%============================================================
%  G2d is one of a set of functions used to evaluate a double
%  integral.  Its purpose is to integrate 'fnc(r,z(i))' over
%  r from R1 to R2, which are either functions of z(i)) or
%  scalars.   This function is called by 'DblIntg'
%============================================================
  z = z(:);
  n = length(z);
  if isstr(R1)==1;
      r1=feval(R1,z);
  else;
      r1=ones(size(z))*R1;
  end
  if isstr(R2)==1;
      r2=feval(R2,z);
  else;
      r2=ones(size(z))*R2;
  end
  for i = 1:n
     f(i) = quadl(fnc,r1(i),r2(i),tl,0,z(i));
  end
  f = f(:);
```

outfun.m

```
function stop = outfun(x,optimValues,state)
%============================================================
%   This function is called from optimize.m after every iteration
%   to check the value of functional.
%   Also it appends the values of all the process parameters
%   and value of functional after each iteration in the file
%   named 'solution.xls'
%============================================================
stop=false;
```

```
sol = [x(1), x(2), x(3), x(4), x(5), optimValues.fval];
dlmwrite('solution.xls',sol,'-append','delimiter','\t','newline','pc');

if optimValues.fval < 0
   stop = true;
end;
```

DeltaVmf.m

```
function r1=DeltaVmf(z)
%=========================================
%  Function DeltaVmf is called from fun.m
%  to evaluate the shear losses at the
%  rigid-plastic deformation boundary Gammamf
%=========================================

global Vi Rpi Rpf Rmi Lpf Lpi Loi Lof Lmi Lmf Rmf;

r = sqrt((z-Lof)*Rmf^2/(Lmf-Lof));
Vrm = -Vi.*Rmi.^2.*r.*(Rmi-Rmf)./(Lmi-Lmf)./(Rmf+(Rmi-Rmf).*z./(Lmi-
Lmf)).^3;
Vzm = -Vi.*Rmi.^2./(Rmf+(Rmi-Rmf).*z./(Lmi-Lmf)).^2;
Vmf = Vi.*Rmi.^2/Rmf.^2;

r1 = abs((Vmf+Vzm).*(((z-Lof).*Rmf.^2./(Lmf-Lof)).^(1./2))-
Vrm.*((1./2).*(Rmf.^2)./(Lmf-Lof)));
```

DeltaVmi.m

```
function r1=DeltaVmi(z)
%=========================================
%  Function DeltaVmi is called from fun.m
%  to evaluate the shear losses at the
%  rigid-plastic deformation boundary Gammami
%=========================================

global Vi Rpi Rpf Rmi Lpf Lpi Loi Lof Lmi Lmf Rmf;

r = sqrt((z-Loi).*Rmi.^2./(Lmi-Loi));
Vrm = -Vi.*Rmi.^2.*r.*(Rmi-Rmf)./(Lmi-Lmf)./(Rmf+(Rmi-Rmf).*z./(Lmi-
Lmf)).^3;
Vzm = -Vi.*Rmi.^2./(Rmf+(Rmi-Rmf).*z./(Lmi-Lmf)).^2;

r1 = abs((Vi+Vzm).*(((z-Loi).*Rmi.^2/(Lmi-Loi)).^(1./2))-
(Vrm.*(0.5.*(Rmi.^2)./(Lmi-Loi))));
```

DeltaVpf.m

```
function r1=DeltaVpf(z)
%=========================================
%  Function DeltaVpf is called from fun.m
%  to evaluate the shear losses at the
%  rigid-plastic deformation boundary Gammapf
%=========================================

global Vi Rpi Rpf Rmi Lpf Lpi Loi Lof Lmi Lmf Rmf;

r = Rpf + (Rmf-Rpf).*z./Lmf;

Vrp = -Vi.*(Rpi.^2-Rmi.^2).*((Rmf+(Rmi-Rmf).*z./(Lmi-Lmf)).*(Rmi-
Rmf)./(Lmi-Lmf).*((Rpf+(Rpi-Rpf).*z./Lpi).^2-r.^2)+(Rpf+(Rpi-
Rpf).*z./Lpi).*(Rpi-Rpf)./Lpi.*(r.^2-(Rmf+(Rmi-Rmf).*z./(Lmi-
Lmf)).^2))./(r.*((Rpf+(Rpi-Rpf).*z./Lpi).^2-(Rmf+(Rmi-Rmf).*z./(Lmi-
Lmf)).^2).^2);
Vzp = -Vi.*(Rpi.^2-Rmi.^2)./((Rpf+(Rpi-Rpf).*z./Lpi).^2-(Rmf+(Rmi-
Rmf).*z./(Lmi-Lmf)).^2);

Vpf = Vi.*(Rpi.^2-Rmi.^2)./(Rpf.^2-Rmf.^2);

r1 = abs(Vpf+Vzp-Vrp.*((Rmf-Rpf)./Lmf)).*(Rpf + (Rmf-Rpf).*z./Lmf);
```

DeltaVpi.m

```
function r1=DeltaVpi(z)
%=========================================
%  Function DeltaVpi is called from fun.m
%  to evaluate the shear losses at the
%  rigid-plastic deformation boundary Gammapi
%=========================================

global Vi Rpi Rpf Rmi Lpf Lpi Loi Lof Lmi Lmf Rmf;

r = (Rmi.*Lpi-Rpi.*Lmi)./(Lpi-Lmi)+(Rpi-Rmi).*z./(Lpi-Lmi);

Vrp = -Vi.*(Rpi.^2-Rmi.^2).*((Rmf+(Rmi-Rmf).*z./(Lmi-Lmf)).*(Rmi-
Rmf)./(Lmi-Lmf).*((Rpf+(Rpi-Rpf).*z./Lpi).^2-r.^2)+(Rpf+(Rpi-
Rpf).*z./Lpi).*(Rpi-Rpf)./Lpi.*(r.^2-(Rmf+(Rmi-Rmf).*z./(Lmi-
Lmf)).^2))./(r.*((Rpf+(Rpi-Rpf).*z./Lpi).^2-(Rmf+(Rmi-Rmf).*z./(Lmi-
Lmf)).^2).^2);
Vzp = -Vi.*(Rpi.^2-Rmi.^2)./((Rpf+(Rpi-Rpf).*z./Lpi).^2-(Rmf+(Rmi-
Rmf).*z./(Lmi-Lmf)).^2);

r1 = abs(Vi+Vzp-Vrp.*((Rpi-Rmi)./(Lpi-Lmi))).*((Rmi.*Lpi-
Rpi.*Lmi)./(Lpi-Lmi)+(Rpi-Rmi).*z./(Lpi-Lmi));
```

DeltaVRm.m

```
function r1=DeltaVRm(z)
%=========================================
%  Function DeltaVRm is called from fun.m
%  to evaluate the frictional losses at the
%  metal polymer interface given by 'Rm'
%=========================================

global Vi Rpi Rpf Rmi Lpf Lpi Loi Lof Lmi Lmf Rmf;

r = Rmf + (Rmi-Rmf).*z./(Lmi-Lmf);
Vrm = -Vi.*Rmi.^2.*r.*(Rmi-Rmf)./(Lmi-Lmf)./(Rmf+(Rmi-Rmf).*z./(Lmi-
Lmf)).^3;
Vzm = -Vi.*Rmi.^2./(Rmf+(Rmi-Rmf).*z./(Lmi-Lmf)).^2;
Vrp = -Vi.*(Rpi.^2-Rmi.^2).*((Rmf+(Rmi-Rmf).*z./(Lmi-Lmf)).*(Rmi-
Rmf)./(Lmi-Lmf).*((Rpf+(Rpi-Rpf).*z./Lpi).^2-r.^2)+(Rpf+(Rpi-
Rpf).*z./Lpi).*(Rpi-Rpf)./Lpi.*(r.^2-(Rmf+(Rmi-Rmf).*z./(Lmi-
Lmf)).^2))./r.*((Rpf+(Rpi-Rpf).*z./Lpi).^2-(Rmf+(Rmi-Rmf).*z./(Lmi-
Lmf)).^2).^2;
Vzp = -Vi.*(Rpi.^2-Rmi.^2)./((Rpf+(Rpi-Rpf).*z./Lpi).^2-(Rmf+(Rmi-
Rmf).*z./(Lmi-Lmf)).^2);

r1 = abs(Vzp-Vzm).*sqrt(1+((Rmi-Rmf)./(Lmi-Lmf)).^2);
```

DeltaVRp.m

```
function r1=DeltaVRp(z)
%=========================================
%  Function DeltaVRp is called from fun.m
%  to evaluate the frictional losses at the
%  die and polymer interface given by 'Rp'
%=========================================

global Vi Rpi Rpf Rmi Lpf Lpi Loi Lof Lmi Lmf Rmf;

r = Rpf + (Rpi-Rpf).*z./Lpi;
Vrp = -Vi.*(Rpi.^2-Rmi.^2).*((Rmf+(Rmi-Rmf).*z./(Lmi-Lmf)).*(Rmi-
Rmf)./(Lmi-Lmf).*((Rpf+(Rpi-Rpf).*z./Lpi).^2-r.^2)+(Rpf+(Rpi-
Rpf).*z./Lpi).*(Rpi-Rpf)./Lpi.*(r.^2-(Rmf+(Rmi-Rmf).*z./(Lmi-
Lmf)).^2))./r.*((Rpf+(Rpi-Rpf).*z./Lpi).^2-(Rmf+(Rmi-Rmf).*z./(Lmi-
Lmf)).^2).^2;
Vzp = -Vi.*(Rpi.^2-Rmi.^2)./((Rpf+(Rpi-Rpf).*z./Lpi).^2-(Rmf+(Rmi-
Rmf).*z./(Lmi-Lmf)).^2);

r1 = abs(Vzp).*sqrt(1+((Rpi-Rpf)./Lpi).^2);
```

Gammamf.m

```
function r2=Gammamf(z)
%=========================================
%  Function Gammamf is called from DblIntg.m
%  to evaluate the value of functional
%  for a particular 'z' at limit of integral
%  Gammamf
%=========================================

global Vi Rpi Rpf Rmi Lpf Lpi Loi Lof Lmi Lmf Rmf;

r2 = sqrt((z-Lof)*Rmf^2/(Lmf-Lof));
```

Gammami.m

```
function r2=Gammami(z)
%=========================================
%  Function Gammami is called from DblIntg.m
%  to evaluate the value of functional
%  for a particular 'z' at limit of integral
%  Gammami
%=========================================

global Vi Rpi Rpf Rmi Lpf Lpi Loi Lof Lmi Lmf Rmf;

r2 = sqrt((z-Loi)*Rmi^2/(Lmi-Loi));
```

Gammapf.m

```
function r2=Gammapf(z)
%=========================================
%  Function Gammapf is called from DblIntg.m
%  to evaluate the value of functional
%  for a particular 'z' at limit of integral
%  Gammapf
%=========================================

global Vi Rpi Rpf Rmi Lpf Lpi Loi Lof Lmi Lmf Rmf;

r2 = Rpf + (Rmf-Rpf)*z/Lmf;
```

Gammapi.m

```
function r2=Gammapi(z)
%=========================================
%  Function Gammapi is called from DblIntg.m
%  to evaluate the value of functional
%  for a particular 'z' at limit of integral
%  Gammapi
%=========================================

global Vi Rpi Rpf Rmi Lpf Lpi Loi Lof Lmi Lmf Rmf;

r2 = ((Rmi*Lpi-Rpi*Lmi)+(Rpi-Rmi)*z)/(Lpi-Lmi);
```

Rm.m

```
function r1=Rm(z)
%=========================================
%  Function Rm is called from DblIntg.m
%  to evaluate the value of functional
%  for a particular 'z' at limit of integral
%  Rm
%=========================================

global Vi Rpi Rpf Rmi Lpf Lpi Loi Lof Lmi Lmf Rmf;
r1 = Rmf + (Rmi-Rmf)*z/(Lmi-Lmf);
```

Rp.m

```
function r2=Rp(z)
%=========================================
%  Function Rp is called from DblIntg.m
%  to evaluate the value of functional
%  for a particular 'z' at limit of integral
%  Rp
%=========================================

global Vi Rpi Rpf Rmi Lpf Lpi Loi Lof Lmi Lmf Rmf;
r2 = Rpf + (Rpi-Rpf)*z/Lpi;
```

Wim.m

```
function f = Wim(r,z)
%=============================================
%  Function Wim is called from DblIntg.m
%  which eventually is called from fun.m
%  to evaluate the functional for calculating
```

```
%  power for internal deformation in metal
%===============================================

global Vi Rpi Rpf Rmi Lpf Lpi Loi Lof Lmi Lmf Rmf;
f = (1./2.*(12.*Vi.^2.*Rmi.^4.*(Rmi-Rmf).^2./(Lmi-Lmf).^2./(Rmf+(Rmi-
Rmf).*z./(Lmi-Lmf)).^6+9.*Vi.^2.*Rmi.^4.*r.^2.*(Rmi-Rmf).^4./(Lmi-
Lmf).^4./(Rmf+(Rmi-Rmf).*z./(Lmi-Lmf)).^8).^(1./2)).*r;
```

Wip.m

```
function f = Wip(r,z)
%===============================================
%  Function Wip is called from DblIntg.m
%  which eventually is called from fun.m
%  to evaluate the functional for calculating
%  power for internal deformation in metal
%===============================================

global Vi Rpi Rpf Rmi Lpf Lpi Loi Lof Lmi Lmf Rmf;
f = (1./2.*(2.*Vi.^2.*(Rpi.^2-Rmi.^2).^2.*((Rpf+(Rpi-
Rpf).*z./Lpi).*(Rpi-Rpf)./Lpi.*(1+(Rmf+(Rmi-Rmf).*z./(Lmi-
Lmf)).^2./r.^2)-(Rmf+(Rmi-Rmf).*z./(Lmi-Lmf)).*(Rmi-Rmf)./(Lmi-
Lmf).*(1+(Rpf+(Rpi-Rpf).*z./Lpi).^2./r.^2)).^2./((Rpf+(Rpi-
Rpf).*z./Lpi).^2-(Rmf+(Rmi-Rmf).*z./(Lmi-
Lmf)).^2).^4+8.*Vi.^2.*(Rpi.^2-Rmi.^2).^2.*((Rpf+(Rpi-
Rpf).*z./Lpi).*(Rpi-Rpf)./Lpi-(Rmf+(Rmi-Rmf).*z./(Lmi-Lmf)).*(Rmi-
Rmf)./(Lmi-Lmf)).^2./((Rpf+(Rpi-Rpf).*z./Lpi).^2-(Rmf+(Rmi-
Rmf).*z./(Lmi-Lmf)).^2).^4+2.*Vi.^2.*(Rpi.^2-Rmi.^2).^2.*((Rmf+(Rmi-
Rmf).*z./(Lmi-Lmf)).*(Rmi-Rmf)./(Lmi-Lmf).*((Rpf+(Rpi-
Rpf).*z./Lpi).^2./r.^2-1)+(Rpf+(Rpi-Rpf).*z./Lpi).*(Rpi-Rpf)./Lpi.*(1-
(Rmf+(Rmi-Rmf).*z./(Lmi-Lmf)).^2./r.^2)).^2./((Rpf+(Rpi-
Rpf).*z./Lpi).^2-(Rmf+(Rmi-Rmf).*z./(Lmi-Lmf)).^2).^4+4.*(-Vi.*(Rpi.^2-
Rmi.^2).*((Rmi-Rmf).^2./(Lmi-Lmf).^2.*((Rpf+(Rpi-Rpf).*z./Lpi).^2-
r.^2)+(Rpi-Rpf).^2./Lpi.^2.*(r.^2-(Rmf+(Rmi-Rmf).*z./(Lmi-
Lmf)).^2)).*((Rpf+(Rpi-Rpf).*z./Lpi).^2-(Rmf+(Rmi-Rmf).*z./(Lmi-
Lmf)).^2).^2+(4.*(Rpf+(Rpi-Rpf).*z./Lpi).*(Rpi-Rpf)./Lpi-4.*(Rmf+(Rmi-
Rmf).*z./(Lmi-Lmf)).*(Rmi-Rmf)./(Lmi-Lmf)).*((Rmf+(Rmi-Rmf).*z./(Lmi-
Lmf)).*(Rmi-Rmf)./(Lmi-Lmf).*((Rpf+(Rpi-Rpf).*z./Lpi).^2-
r.^2)+(Rpf+(Rpi-Rpf).*z./Lpi).*(Rpi-Rpf)./Lpi.*(r.^2-(Rmf+(Rmi-
Rmf).*z./(Lmi-Lmf)).^2)).*((Rpf+(Rpi-Rpf).*z./Lpi).^2-(Rmf+(Rmi-
Rmf).*z./(Lmi-Lmf)).^2).^3).^2).^(1./2)).*r;
```

APPENDIX II

A simplex is a geometrical figure formed by set of points (n+1) in n-dimensional space. Thus the simplest example of simplex is a triangle in two dimensional space. The initial guess is vector X_i and assigning it to first vertex X_1 and the other two vertices are determined by $X_2 = X_i+\lambda i$ and $X_3 = X_i+\lambda j$. Hence a triangular simplex with its vertices being X_1, X_2 and X_3 as the initial simplex is constructed for optimizing the objective functional f. The objective function is evaluated at these three vertices of simplex and the algorithm replaces one of the vertex at each iteration in the direction of decreasing f. The flow chart of algorithm is given in Figure 26 and it follows following steps:

- If the objective function has highest value at vertex X_h then the point X_r can be found by reflecting the triangular simplex in the opposite direction. The new simplex is made by including X_1, X_2 and X_r and this process is reflection.
- Reflection is done along a line from X_h through the midpoint of the opposite face of the triangle X_o. If the functional at reflected point X_r founds a lower value algorithm tries a larger move along the same direction and is called as expansion. Expansion coefficient is given by γ. If the functional is not lower a new X_h has been found and new reflection can be carried out. Repeating the process of finding a new X_h and reflecting goes on until the simplex reaches the optimum.
- If reflection process gives a X_r such that $f(X_r) > f(X_i)$ for all i except $i=h$ and $f(X_r) < f(X_h)$ then X_h is replaced by X_r and simplex is contracted towards lowest point and reflection process is resumed. Contraction coefficient is given by β.

APPENDIX III

Since ABAQUS does not provides any parametric study through it's built in interactive session or through any control card hence a python script was generated to conduct parametric study. Given below is a file with extension '.psf' which is the python script.

test1-0724_coated_extrusion_para.psf

```
#
##################################################################################
#  THIS SCRIPT RUNS A SEQUENCE OF PARAMETRIZED INPUT FILES TO
#  STUDY THE EFFECT OF DIFFERENT DIE ANGLES FOR A GIVEN
#  REDUCTION RATIO ON REACTION FORCE/EXTRUSION PRESSURE
#  REQUIRED.
##################################################################################
#
study = ParStudy(par=('x_coord_1', 'y_coord_1'), name='test1-
0724_coated_extrusion_para')

#  DEFINE THE PARAMETERS

study.define (DISCRETE, par='y_coord_1', domain=(-0.06430052, -
0.00671282, 0.01267949, 0.02252523, 0.02855493, 0.03267949, 0.03571852,
0.03808246, 0.04000000))
study.define(DISCRETE, par='x_coord_1', domain=(0.09))

#  SAMPLE THE PARAMETERS - INPUT THE APPROPRIATE VALUES

study.sample(INTERVAL, par='y_coord_1', interval=-2)
study.sample(INTERVAL, par='x_coord_1', interval=-2)

#  COMBINE THE SAMPLES INTO ANALYSES

study.combine(MESH, name='dset90')

#  GENERATE INPUT DECKS AND EXECUTION SCRIPT
#  FOR VARIOUS TEMPLATES

study.generate(template='test1-0724_coated_extrusion_para')

#  EXECUTE RUNS SEQUENTIALLY

study.execute(ALL)
```

The corresponding ABAQUS input file i.e. file with extension '.inp' for the above given python script is given below. Note the nodes and elements details is missing and only control elements and parametric geometry details are given below -

test1-0724_coated_extrusion_para.inp

```
*Heading
** Job name: test2-0718_coated_extrusion Model name: Model-2
*Preprint, echo=NO, model=NO, history=NO, contact=NO
**
** PARTS
**
*Part, name=Coating
*End Part
*Part, name=Die
*End Part
*Part, name=Rod
*End Part
**
** ASSEMBLY
**
*Assembly, name=Assembly
**
*Instance, name=Die-1, part=Die
** Region: (Section-2:Picked)
*Element, type=MASS, elset=_PickedSet3_MASS_
1, 1
*Mass, elset=_PickedSet3_MASS_
1e+10,
**
** Parametric Input Reduction Ratio fixed and angle is varying
**
*Parameter
x_coord_1 = 0.05
y_coord_1 = -0.01
x_coord_2 = x_coord_1
y_coord_2 = y_coord_1 - 0.025
x_coord_3 = x_coord_2 + 0.025
y_coord_3 = y_coord_2
x_coord_4 = x_coord_3
*Node
      1,          0.3,         -0.2,           0.
*Nset, nset=Die-1-RefPt_, internal
1,
*Surface, type=SEGMENTS, name=RigidSurface_, internal, FILLET=0.075
START,          0.3,         -0.2
 LINE,      <x_coord_4>,     -0.2
 LINE,      <x_coord_3>,     <y_coord_3>
 LINE,      <x_coord_2>,     <y_coord_2>
```

```
 LINE,      <x_coord_1>,     <y_coord_1>
 LINE, 0.0999999999999998, 0.0599720518009124
 LINE,          0.1,          0.4
 LINE,          0.3,          0.4
 LINE,          0.3,         -0.2
*Rigid Body, ref node=Die-1-RefPt_, analytical surface=RigidSurface_
*End Instance
**



**
** ELEMENT CONTROLS
**
*Section Controls, name=EC-1, hourglass=ENHANCED
1., 1., 1.
*Section Controls, name=EC-2, hourglass=ENHANCED
1., 1., 1.
**
** MATERIALS
**
*Material, name="Metal - Rod"
*Density
2700.,
*Elastic
 6.9e+10, 0.33
*Plastic
    6e+07,    0.
    9e+07, 0.125
 1.13e+08,  0.25
 1.24e+08, 0.375
 1.33e+08,   0.5
 1.65e+08,    1.
 1.66e+08,    2.
*Material, name=Plastic-Coating
*Density
1400.,
*Elastic
 8.9e+09, 0.33
*Plastic
 8e+07,    0.
 8e+07, 0.125
 8e+07,  0.25
 8e+07, 0.375
 8e+07,   0.5
 8e+07,    1.
 8e+07,    2.
**
** INTERACTION PROPERTIES
**
*Surface Interaction, name=friction
*Friction, shear traction slope=0.5
 0.1,
** ----------------------------------------------------------------
```

```
**
** STEP: Step-1
**
*Step, name=Step-1
Extrusion
*Dynamic, Explicit
, 20.
*Bulk Viscosity
0.06, 1.2
** Mass Scaling: Semi-Automatic
**               Whole Model
*Fixed Mass Scaling, factor=1000000.
**
** BOUNDARY CONDITIONS
**
** Name: Top Velocity Type: Velocity/Angular velocity
*Boundary, type=VELOCITY
_PickedSet40, 2, 2, -0.01
** Name: axis Type: Symmetry/Antisymmetry/Encastre
*Boundary
_PickedSet11, XSYMM
** Name: fixed Type: Symmetry/Antisymmetry/Encastre
*Boundary
_PickedSet61, ENCASTRE
*Adaptive Mesh Controls, name=Adaptive-1
1., 0., 0.
*Adaptive Mesh, elset=Combined_Rod+Coating, controls=Adaptive-1,
frequency=25, initial mesh sweeps=100, mesh sweeps=10, op=NEW
**
** INTERACTIONS
**
** Interaction: Int-2
*Contact Pair, interaction=friction, mechanical constraint=KINEMATIC,
cpset=Int-2
Die-1.RigidSurface_, _PickedSurf55
** Interaction: Interaction-1
*Contact Pair, interaction=friction, mechanical constraint=KINEMATIC,
cpset=Interaction-1
Die-1.RigidSurface_, _PickedSurf52
*Contact Controls, cpset=Interaction-1
**
** OUTPUT REQUESTS
**
*Restart, write, number interval=1, time marks=NO
**
** FIELD OUTPUT: F-Output-1
**
*Output, field, variable=PRESELECT
**
** HISTORY OUTPUT: H-Output-1
**
*Output, history, variable=PRESELECT
*End Step
```

VITA

Name: Ritesh Lalit Shah

Address: c/o Dr. Jyhwen Wang
Department of Mechanical Engineering,
Engineering Physics Building,
Texas A&M University,
College Station, TX 77843-3123

Email Address: riteshshah@tamu.edu

Education: B.E., Mechanical Engineering, College of Engineering, Pune, India 2002
M.S., Mechanical Engineering, Texas A&M University, 2006